142

0-315-12456-3

National Library of Canada | Bibliothèque nationale du Canada

Canadian Theses Division | Division des thèses canadiennes

Ottawa, Canada
K1A 0N4

60367

PERMISSION TO MICROFILM — AUTORISATION DE MICROFILMER

• Please print or type — Écrire en lettres moulées ou dactylographier

Full Name of Author — Nom complet de l'auteur

STEPHEN KAM-LING CHIU

Date of Birth — Date de naissance

Oct 8, 1954

Country of Birth — Lieu de naissance

HONG KONG

Permanent Address — Résidence fixe

16 RUA DO BOCAGE MACAO (VIA HONG KONG)

Title of Thesis — Titre de la thèse

CRUSTAL ~~STR~~ STRUCTURE BENEATH VANCOUVER ISLAND

University — Université

UNIV. OF ALBERTA

Degree for which thesis was presented — Grade pour lequel cette thèse fut présentée

M. Sc

Year this degree conferred — Année d'obtention de ce grade

1982

Name of Supervisor — Nom du directeur de thèse

G. L. CUMMING

Permission is hereby granted to the NATIONAL LIBRARY OF CANADA to microfilm this thesis and to lend or sell copies of the film.

The author reserves other publication rights, and neither the thesis nor extensive extracts from it may be printed or otherwise reproduced without the author's written permission.

L'autorisation est, par la présente, accordée à la BIBLIOTHÈQUE NATIONALE DU CANADA de microfilmer cette thèse et de prêter ou de vendre des exemplaires du film.

L'auteur se réserve les autres droits de publication; ni la thèse ni de longs extraits de celle-ci ne doivent être imprimés ou autrement reproduits sans l'autorisation écrite de l'auteur.

Date

July 16, 82

Signature

Kam Ling Chiu

NL-91 (4/77)

CANADIAN THESES ON MICROFICHE

I.S.B.N.

THESES CANADIENNES SUR MICROFICHE

National Library of Canada
Collections Development Branch

Canadian Theses on
Microfiche Service

Ottawa, Canada
K1A 0N4

Bibliothèque nationale du Canada
Direction du développement des collections

Service des thèses canadiennes
sur microfiche

NOTICE

The quality of this microfiche is heavily dependent upon the quality of the original thesis submitted for microfilming. Every effort has been made to ensure the highest quality of reproduction possible.

If pages are missing, contact the university which granted the degree.

Some pages may have indistinct print especially if the original pages were typed with a poor typewriter ribbon or if the university sent us a poor photocopy.

Previously copyrighted materials (journal articles, published tests, etc.) are not filmed.

Reproduction in full or in part of this film is governed by the Canadian Copyright Act, R.S.C. 1970, c. C-30. Please read the authorization forms which accompany this thesis.

THIS DISSERTATION
HAS BEEN MICROFILMED
EXACTLY AS RECEIVED

AVIS

La qualité de cette microfiche dépend grandement de la qualité de la thèse soumise au microfilmage. Nous avons tout fait pour assurer une qualité supérieure de reproduction.

S'il manque des pages, veuillez communiquer avec l'université qui a conféré le grade.

La qualité d'impression de certaines pages peut laisser à désirer, surtout si les pages originales ont été dactylographiées à l'aide d'un ruban usé ou si l'université nous a fait parvenir une photocopie de mauvaise qualité.

Les documents qui font déjà l'objet d'un droit d'auteur (articles de revue, examens publiés, etc.) ne sont pas microfilmés.

La reproduction, même partielle, de ce microfilm est soumise à la Loi canadienne sur le droit d'auteur, SRC 1970, c. C-30. Veuillez prendre connaissance des formules d'autorisation qui accompagnent cette thèse.

LA THÈSE A ÉTÉ
MICROFILMÉE TELLE QUE
NOUS L'AVONS REÇUE

NL-339 (r. 82/08)

Canada

THE UNIVERSITY OF ALBERTA

CRUSTAL STRUCTURE BENEATH VANCOUVER ISLAND FROM REFRACTION DATA

by

STEPHEN KAM-LING CHIU

A THESIS

SUBMITTED TO THE FACULTY OF GRADUATE STUDIES AND RESEARCH

IN PARTIAL FULFILMENT OF THE REQUIREMENTS FOR THE DEGREE

OF MASTER OF SCIENCE

IN

GEOPHYSICS

DEPARTMENT OF PHYSICS

EDMONTON, ALBERTA

FALL 1982

THE UNIVERSITY OF ALBERTA

RELEASE FORM

NAME OF AUTHOR STEPHEN KAM-LING CHIU

TITLE OF THESIS CRUSTAL STRUCTURE BENEATH VANCOUVER ISLAND FROM REFRACTION DATA

DEGREE FOR WHICH THESIS WAS PRESENTED MASTER OF SCIENCE

YEAR THIS DEGREE GRANTED FALL 1982

Permission is hereby granted to THE UNIVERSITY OF ALBERTA LIBRARY to reproduce single copies of this thesis and to lend or sell such copies for private, scholarly or scientific research purposes only.

The author reserves other publication rights, and neither the thesis nor extensive extracts from it may be printed or otherwise reproduced without the author's written permission.

(SIGNED) Kam Ling Chiu

PERMANENT ADDRESS:

803-A, 4th Street S.E.,

Medicine Hat, Alberta

T1A 0L7

DATED July 15 1982

THE UNIVERSITY OF ALBERTA

FACULTY OF GRADUATE STUDIES AND RESEARCH

The undersigned certify that they have read, and recommend to the Faculty of Graduate Studies and Research, for acceptance, a thesis entitled CRUSTAL STRUCTURE BENEATH VANCOUVER ISLAND FROM REFRACTION DATA submitted by STEPHEN KAM-LING CHIU in partial fulfilment of the requirements for the degree of MASTER OF SCIENCE in GEOPHYSICS.

.....G.h. Cumming.....

Supervisor

.....A. J. Cote.....

.....R. S. Lambert.....

.....

Date..July 6, 82.....

ABSTRACT

Refraction data along the structural axis of Vancouver Island were recorded as part of the 1980 Vancouver Island Seismic Project. The refraction line extends about 330 km from the southern to the northern end of the island. These partially reversed data were interpreted by the analysis of first arrivals in terms of a horizontal, plane-layered model and also using a WHB inversion of travel times. Synthetic seismograms were also computed in an attempt to match possible Moho reflections.

Interpretation of these data suggests an increasing velocity from 5.30 km/s at the surface to 6.5 km/s at 5 km depth, and a more gradual increase to 7.0 km/s at 17 km depth. Discontinuity of the travel-time curve on the Fuca profiles has been interpreted as evidence of a low velocity zone in the lower crust. Although probable Pn arrivals from the Moho were observed, its depth and shape remain uncertain. However, an interpretation that fits the observed refraction data from the crust and reflection data from the Moho by synthetic modelling, has a Moho depth of 44 km and a mantle velocity of 8.0 km/s. Lateral variation of thicknesses is significant beneath the central part of Vancouver Island. The analysis of first arrivals based on the limited refraction data makes the interpretation somewhat arbitrary, thus the proposed model is only speculative at the present time.

ACKNOWLEDGEMENTS

I wish to sincerely thank Dr. G.L. Cumming for his work, guidance, and encouragement throughout the entire programme.

Mr. Charles McCloughan offered many constructive suggestions during the preparation of seismic records. His invaluable help is greatly appreciated.

I would like to express my gratitude to the CO-CRUST group, and many other persons who assisted in the 1980 field operation.

Special thanks are extended to Dr. F. Hron who did the synthetic modelling in Chapter five.

This thesis is dedicated to my parents who have given financial and emotional support throughout my career.

During the course of this research, the author was supported by a Graduate Teaching Assistantship from the Department of Physics, University of Alberta.

Table of Contents

List of Tables

List of Figures

1. INTRODUCTION

The study of transmission of elastic waves through the earth has been one of intensive research in geophysics over the past few decades. Seismology provides the tools for studying the structure and composition of the earth's interior. Seismic evidence has shown that the crust of the earth is about 50 km thick under continents and 5 km under the oceans; a distinct worldwide discontinuity called the 'Moho' (the Mohorovicic discontinuity), which has the characteristics of strong seismic velocity variations, divides the crust from the upper mantle.

In Canada, deep crustal studies started in 1947 (Hodgson, 1947). Recently ten groups from Universities and Government have carried on a long-term seismic program to study the crust and upper mantle over different regions. Some examples of the studies that were done included: Cumming and Kanasewich (1966); Rankin, Ravindra and Zwicker(1969); Mereu and Hunter(1969); Overton (1970); Barr(1971); Hales and Nation (1973); Berry and Forsyth(1975); Cumming, Clowes, and Ellis(1979).

A review of the published interpretations leads to a general crustal structure in Canada (Berry,1973):

1. Pn velocities (Compressional wave velocities under the Moho discontinuity) vary from a value possibly as low as 7.7 km/sec under Vancouver Island to 8.6 km/sec and higher in the extreme eastern part of the shield and some parts of Atlantic coast.

2. Large areas of Canada have a crustal thickness of 30-40 km, with Vancouver Island, the southwestern Prairies, the Lake Superior basin and parts of the eastern shield of Quebec being thicker.
3. The Riel discontinuity, a deep intra-crustal reflector and sometimes a refractor, is widely reported in the Prairies, and Arctic polar continental shelf. It is not seen in Hudson Bay, nor under Lake Superior, nor in Maritime regions.

This investigation is part of large scale seismic program (VISP 80) which consists of both seismic refraction and reflection experiments in the region of Vancouver Island. The overall objective of this seismic program is to explore the nature of the crust and upper mantle in the transition zone from the Pacific Ocean through Vancouver Island to the mainland of British Columbia.

The present study has the following purposes:

1. Develop crustal velocity-depth functions for refraction data collected from Vancouver Island.
2. Utilize these velocity-depth functions for interpretation of Vancouver Island crustal structure, and provide a control point on the cross refraction profiles which will be interpreted by others.

2. BACKGROUND GEOLOGY AND GEOPHYSICS

2.1 Generalized Geology of Vancouver Island

Vancouver Island is located in the Insular Belt of western British Columbia. The Insular Belt is a series of complexes of largely igneous (volcanic) origin, believed to have formed as part of an island arc system in early Mesozoic time. They are probably allochthonous (Monger and Price, 1979). The events of mountain-building in Mesozoic time had a significant impact on the formation of Vancouver Island. These events involved widespread folding, faulting, and the intrusion of batholiths in the Insular Belt itself, the Coast Mountains, and the Intermontane Belt.

Vulcanism on Vancouver Island, in the form of basaltic lava-flows was extensive during the Mesozoic age. As a result, thick sequences of volcanic rocks of oceanic crustal and island arc type occur throughout the island. Erosion and differential uplift continued to the end of the Tertiary period. The complex history of Vancouver Island has resulted in a great variety of volcanic, plutonic, sedimentary, and metamorphic rocks which result in a high variability of near surface lithologies (Muller, 1974, 1977). However, these rocks are in general of comparatively high density and highly indurated and as a consequence, near surface seismic velocities are relatively high, compared for example to the plains of Western Canada.

2.2 Tectonic Setting of Vancouver Island

The essential features of plate tectonic environment in coastal British Columbia are dominated by the relative motion of three main lithospheric plates: the large Pacific and America plates, and the Juan de Fuca plate. A small northern part of the Fuca plate, which has been named the Explorer plate, has been shown to be moving independently. Fig.2.1 shows the tectonic map in this area. Two distinct features are present along the continental margin: (Keen and Hyndman, 1979)

1. From the southern end of the Vancouver Island to just south of Queen Charlottle Islands there is convergence with subduction of ocean crust beneath the continent.
2. From the Queen Charlottle Islands to southern Alaska there is a transform strike-slip fault separating the Pacific and America plates.

The motion between the Juan de Fuca and Explorer plates occurs across the Nootka transform fault zone, which extends northeasterly from the north end of the Fuca ridge to the continental shelf off north-central Vancouver Island. The active portion of the fault zone, about 20 km wide, has produced extensive disturbance in the 0.5 to 1 km of overlying sediments. Hyndman, Riddihough, and Herzer (1979) showed that the magnetic anomaly pattern required the fault to have a strike-slip motion of about 3 cm/yr, with subduction at the margin being more rapid to the south than to the north of the fault zone.

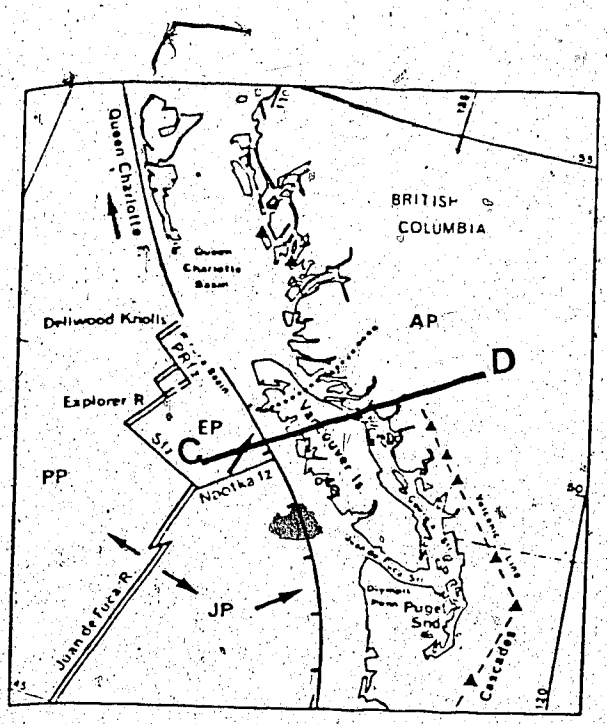

Figure 2.1 Tectonic map of western Canada showing the main lithosphere plate boundaries and relative plate motions. The dotted line is the estimated northern edge of the Juan de Fuca plate. PRfz=Paul Revere fracture zone; Sfz=Sovanco fracture zone; PP=Pacific plate; EP=Explorer plate; JP=Juan de Fuca plate; AP=America plate. (modified from Keen and Hyndman, 1979)

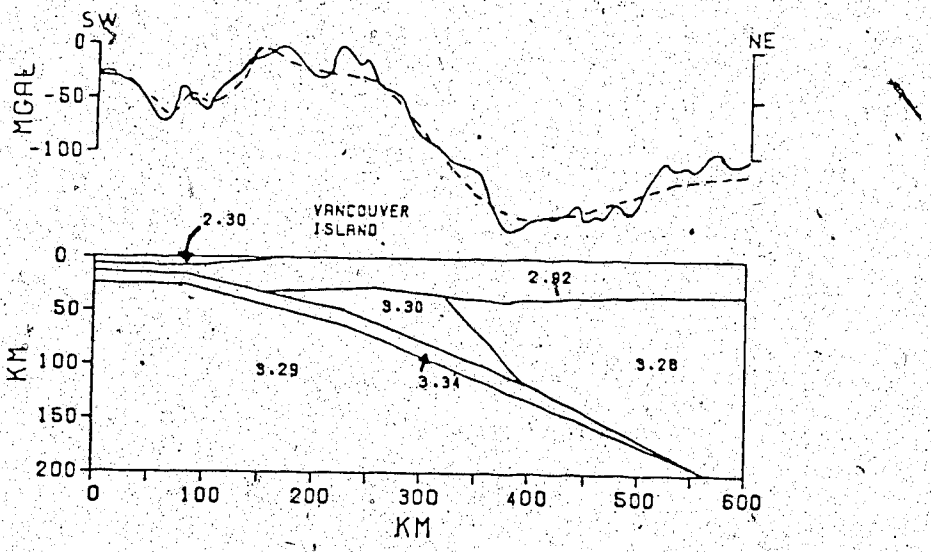

Figure 2.2 Structural section along line CD in Fig. 2.1. Gravity profiles are free air over sea and Bouguer over land; solid=observed, dashed=computed. Density, in $g.cm^{-3}$. (after Riddihough, 1979)

Most subduction zones in other regions are characterized by a deep trench, but there is no such deep trench in this region. With the evidence of a lack of a deep margin trench and deep earthquakes in this zone, Riddihough (1978) suggested that the subduction might be a very recent geological feature, and the absence of a deep trench was probably due to high sedimentation rates and the damming effect of the Juan de Fuca Ridge lying only a few 100 km offshore.

Compressional folding and uplift of Tertiary sediments are also consistently observed along the coast regions, and in detail a model of imbricate thrusting along the continental margin fits the pattern of deformation closely. Detailed experiments along the continental margin attempting to locate microseismicity, have proved negative. However, there is a strong concentration of seismicity of magnitudes up to 6 on the Richter scale in the southern Georgia Strait-Puget Sound area. The larger events generally are deeper than normal, most at about 50 km. Crosson (1972), Roger(1979), Keen and Hyndman(1979) concluded, from the earthquake study, that there were two distinct groups of earthquakes: a shallow group and a second deeper group. An inclined zone, dipping at a shallow angle and along which oceanic lithosphere is supposedly subducting, was postulated to divide the two groups of earthquakes. Thus the concentration of earthquakes in the Georgia Strait region indicates that oceanic lithosphere moves under the

continental margin at a shallow angle until the region of Georgia Strait and Puget Sound, then dips steeply about 10 to 15 degrees down to the mantle.

Heat flow and gravity patterns provide additional evidence of subduction in this region. The heat-flow has the characteristic pattern of a subduction zone: a band of low heat flow extends from the trench to the volcanic arc, and a much higher than normal heat flow extends for a considerable distance inland (McKenzie and Sclater 1968; Hyndman, 1976). The low zone is produced by the cold oceanic lithosphere that sinks beneath the continent; the high heat flow farther inland probably results from the sinking slab. The gravity anomaly exhibits a similar characteristic pattern of two pairs of low and high bands, as shown in Fig. 2.2. The main inland band reflects the established axis of subduction of the Juan de Fuca plate; the weaker band at the continental margin appears in part to be produced by the effect of the boundary between thin oceanic and thick continental crust.

Riddihough (1979) developed a detailed structural model from gravity data. Fig.2.2 shows his model across northern Vancouver Island. The model suggests that oceanic lithosphere is descending, bending and disappearing near the base of the continental slope, and that the crust under Vancouver Island is between 20 to 30 km depth and is underlain by anomalous high density material to produce the observed gravity field. On the whole, all geophysical evidences strongly support the existence of the subduction

zone in southwest British Columbia.

2.3 Previous Seismic experiments

Vancouver Island has been the subject of considerable geophysical investigations. The early structural interpretation was based on the refraction work of White and Savage (1965), and time-term analysis of the same data by Tseng (1968). White and Savage suggested an unusually thick crustal section under Vancouver Island with the Moho lying at a depth of 50 km and with a Pn velocity of 7.7 km/s. Tseng obtained a similar crustal thickness, but he introduced an intermediate layer at a depth of 25 km with a P-wave (compressional wave) velocity of 7.1 km/s.

Berry and Forsyth (1975) attempted to reconcile their data with earlier work. Their data indicated a major discontinuity in the travel-time curve between the mainland coast and Vancouver Island. This major discontinuity is likely to represent a zone of scattering for seismic energy in that region. They also found a thick crust of about 50 km and an intermediate layer at about 30 km under Vancouver Island. Furthermore, analysis of surface waves by Wicken(1977) concluded that two velocity discontinuities existed at about these depths. He indicated that inconsistencies between the model values for Love and Rayleigh waves were suggestive of upper mantle anisotropy.

However, from the analyses of P-S conversions of long-period teleseismic P-waves recorded at the southern end of Vancouver Island, Langston(1981) suggested that there were two Moho discontinuities in this region. The first Moho was at a depth of 20 km, in which the material at this depth represented a remnant of high density upper mantle, and the second was at a depth of 45 km in which the Moho was interpreted as the subducting oceanic crust of the Juan de Fuca plate. A low velocity zone between 20 km and 45 km was also postulated to divide the two Moho discontinuities. If the low velocity zone exists in this region, it would no doubt create difficulties in interpretation of refraction work.

Riddihough(1979) provided a summary of all seismic and gravity interpretations beneath Vancouver Island. A feature of these interpretations is the presence of two discontinuities, one near 30 km depth and one at between 40 to 50 km depth. The crustal thickness determined by seismic methods is significantly different from that deduced by gravity data. To reconcile the conflicts between two interpretations, Riddihough suggested that the subducting oceanic crust of the Juan de Fuca plate beneath Vancouver Island was between 30 to 50 km. The material of this subduction zone has a special feature of having high density and low P-wave velocity. Fig.2.3 shows the P-wave velocity-depth interpretations proposed in a number of these studies. The wide range of the interpretations in Fig. 2.3

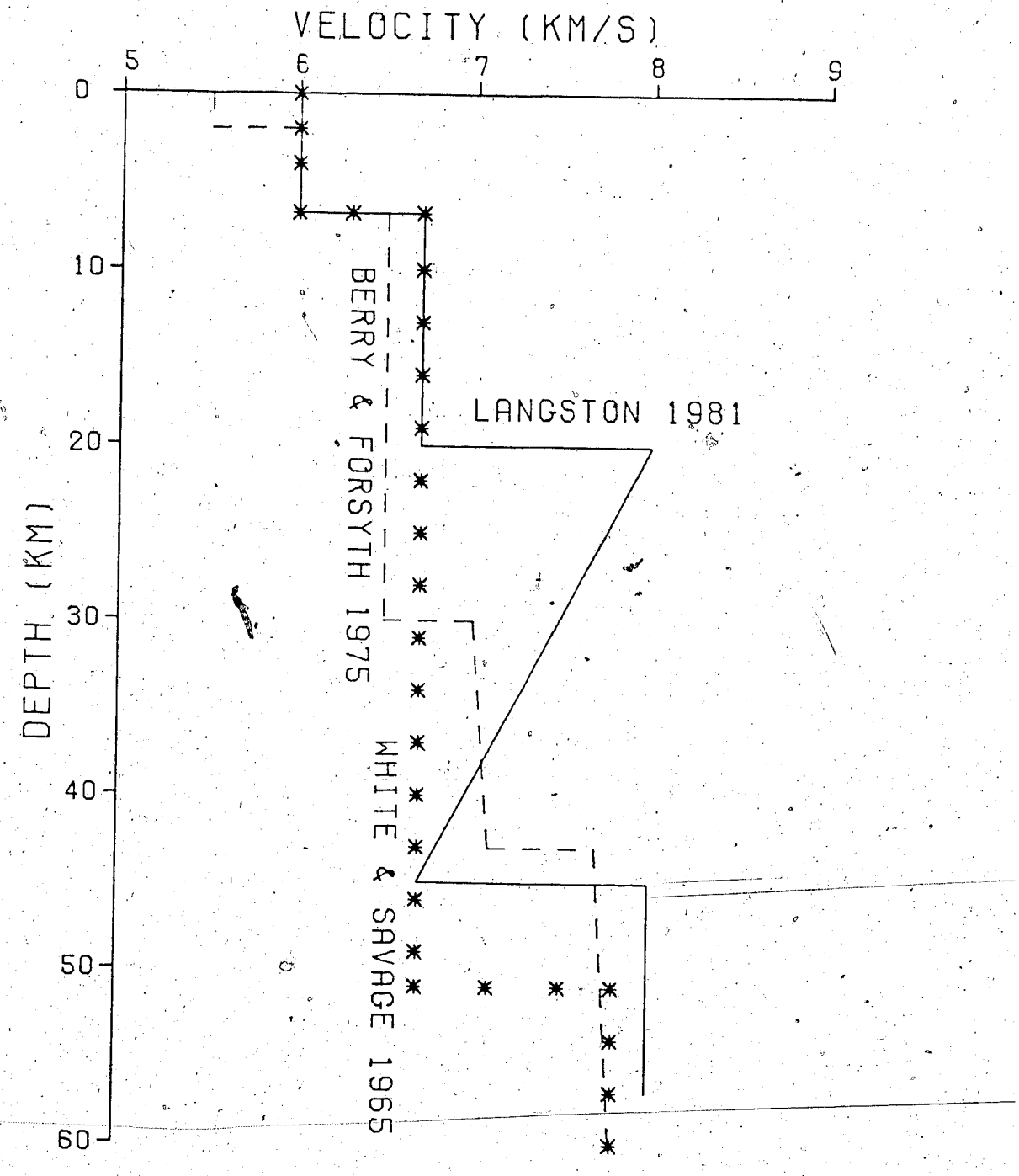

Figure 2.3 P-wave velocity profiles. These are the results of some previous studies of structure beneath Vancouver Island and adjacent regions in the United States: solid line= Langston, dashed line= Berry & Forsyth, stars= White & Savage. (after McMechan and Spence, 1982)

suggests that either the data are ambiguous or there are significant lateral variations in structure beneath Vancouver Island.

The seismic data existing prior to this project do not define clearly the structural characteristics of the crust and upper mantle in this region. The present study is part of a continuing investigation aimed at clarifying the structure under Vancouver Island.

3. DATA ACQUISITION

3.1 Location of Refraction Lines

In August 1980 the CO-CRUST group conducted a field program on Vancouver Island, and included workers from the Universities of British Columbia, Alberta, Saskatchewan, Manitoba and Western Ontario, and the Department of Energy, Mines and Resources of Ottawa. The initial phase of the experiment consisted of refraction measurements undertaken in the period August 9 to 21 followed by a reflection experiment from August 22 to 26.

The data for the present study consist of two refraction lines, NA and AF in Fig.3.1. The distance between the two outermost locations, N and F is approximately 330 km. The centre of the refraction line is located at A. Initially 38 seismic systems were distributed along the 150 km section N-A. Shots A1, N1, and F1 were then detonated at A,N,F respectively. The seismometers were relocated along 180 km of the line A-F for the observation of shots F2, A2, and N2 at F, A, N respectively.

Each of these six profiles is referred to by a name consisting of a shot point designation (N,A, or F) followed by a number '1' or '2'. '1' refers to the northern profile; '2' to the southern profile. For example, profile N1 refers to a shot at N recorded along the northern line NA. The charge size for six shots varied from 900 to 1800 kg. The

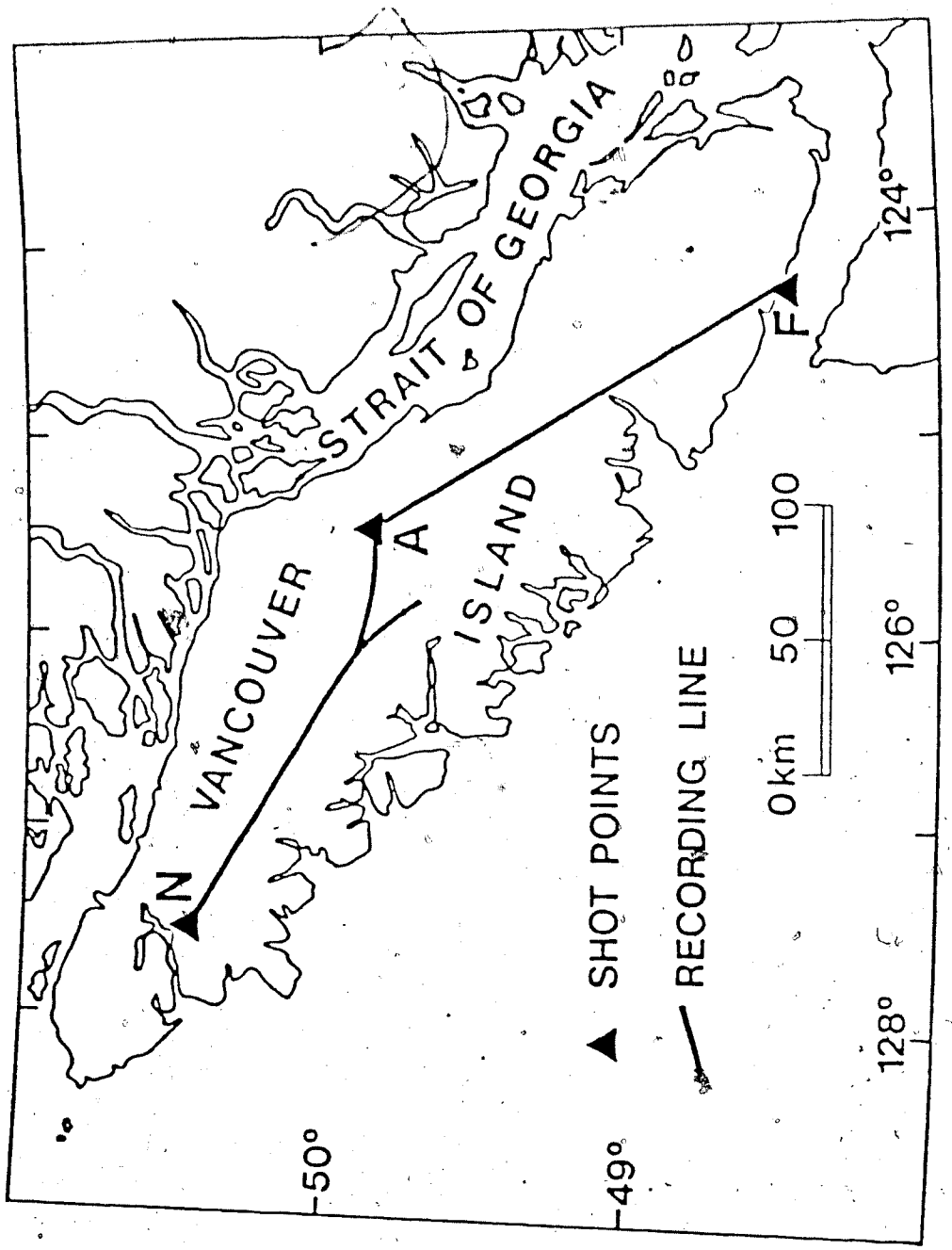

Figure 3.1 VISP 80 Location map. The data are from three shot points N, A, and F. Portable seismometers were placed along the solid lines at an average spacing of about 5 km.(from McMechan and Spence, 1982)

distant shots were 1800 kg; the nearer shots, 900 kg. For details of shot point parameters, the reader is referred to Ellis and Clowes (1981,p.12).

3.2 Data Characteristics on Tape

All refraction data were recorded on magnetic tape by eight different types of recording systems, five digital and three analog. Each system has its own characteristic gain and frequency response to record seismic signals over a passband from 1 to 20 Hertz. Ellis and Clowes(1981,p.20) discussed the details of each system. Each seismometer recorded at least 60 seconds of signals after the first arrival of energy. WWVB signals were also recorded at both the recording site and shotpoint to maintain time control.

All field data were redigitized at a rate of 60 Hz with variations in analog tape speeds taken into consideration. Each record contains 7200 samples, and the first three data words provide information concerning receiver number, shot number, and orientation of the seismometer. The data were written in format (5E16.6) with a block length of 1200 samples (4800 bytes). Thus each event consists of 6 blocks of data on the magnetic tape. To convert all the data to a common ground velocity, each recording has been modified by a gain factor which reflects the various sensitivies of the seismometers and the gain setting of the recording amplifiers.

3.3 Instrumentation of the University of Alberta

In 1980 the seismic array recording system of University of Alberta had twelve channels to record seismic data and two additional channels to record shot instant from a radio receiver and absolute time from WWVB. All data were recorded on a Peripheral Equipment Corporation model 7830-9 digital tape recorded at a tape velocity of 6.25 inches per second, yielding a transfer rate of 5000 bytes per second. (Alsopp, Burke, and Cumming 1972)

The impulse response of the recording instrument and seismometer can be derived from an S-plane representation (Dickens, 1973). The constants in the S-plane representation of both recording system and seismometer may be found by examining the specification of their circuits and their components. Then, these nominal values may be adjusted slightly so that the amplitude and phase spectra calculated from the specifications match the amplitude and phase spectra determined experimentally. The constants in the S-plane representation were derived by G.L. Cumming according to this procedure (in Appendix). Fig. 3.2 and 3.3 show the amplitude and phase spectra of the amplifier system and seismometer which were derived from the S-plane representation.

The amplifier has a flat response from 0.1 Hz to 50 Hz, and the response of the seismometer increases as the frequency increases. Alsopp, Burke, and Cumming (1972) showed that the U. of A. recording system with a bandpass of

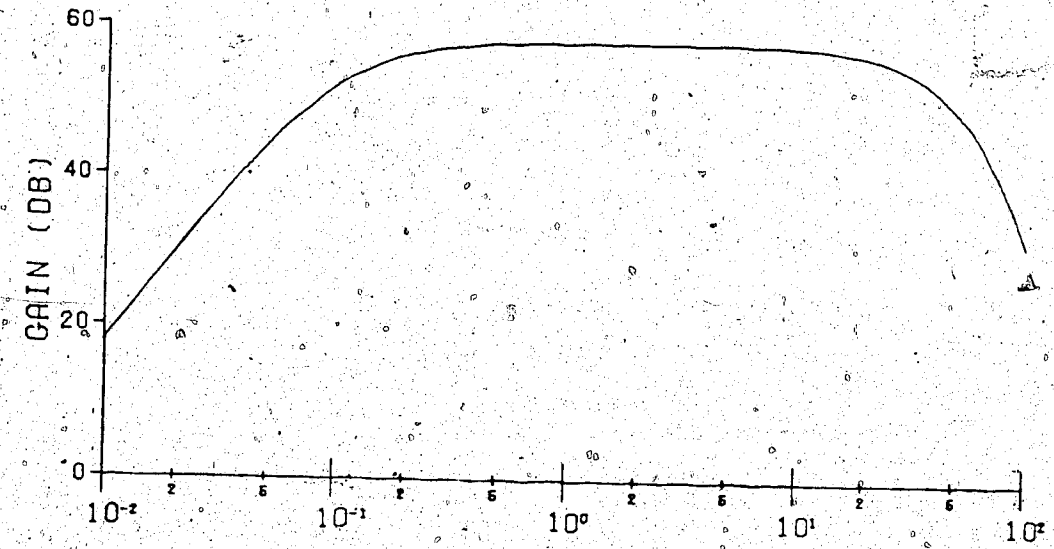

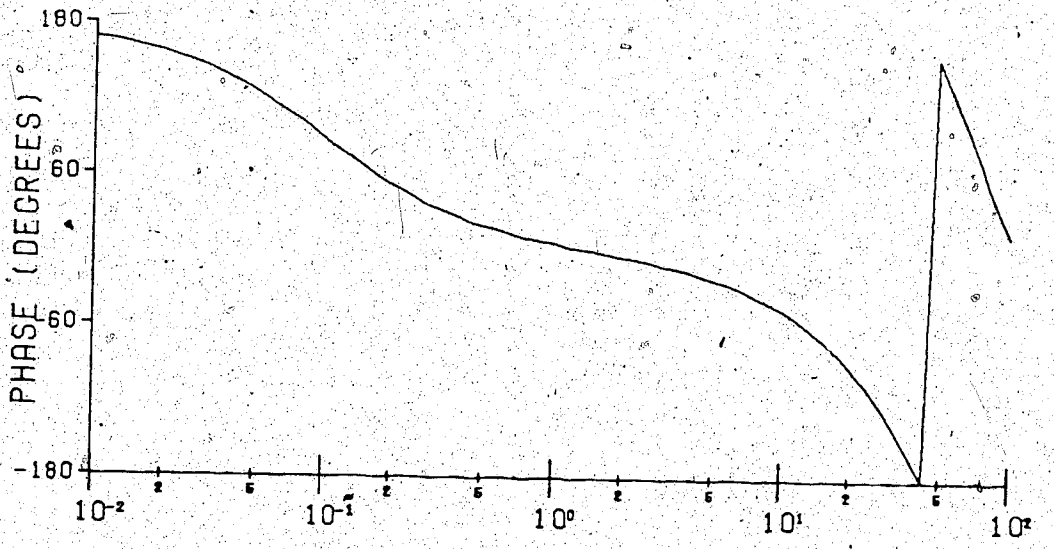

Figure 3.2 Amplitude and phase spectra of the seismic array recording instrument used by the University of Alberta in 1980.

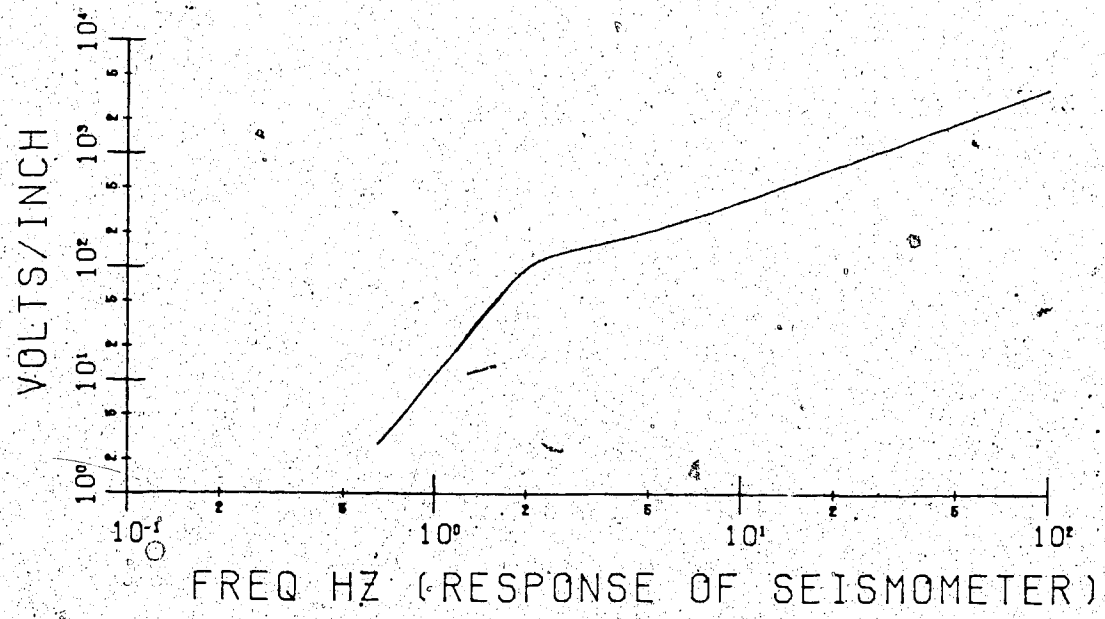

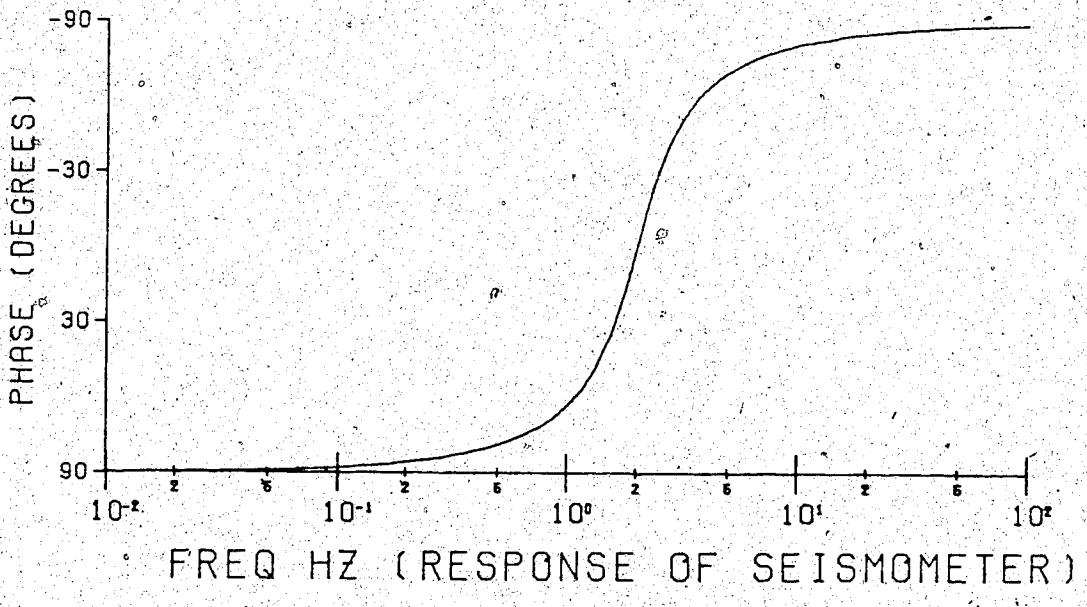

Figure 3.3 Amplitude and phase spectra of the seismometer used by the University of Alberta in 1980.

0.1 to 50 Hz coupled with a 14-bit A to D converter would provide the wide-frequency response and dynamic range for high-quality recording of seismic reflection/ refraction signals from the deep crust, and that the system noise was not a significant factor in data analysis.

Furthermore, the U. of A. digital array offers additional advantages by comparison with a single channel seismometer:

1. An array of detectors reduces the possibility of recording failure compared to a system using a single seismometer.
2. The combination of individual records in the array improves the signal-to-noise ratio. The signal-to-noise ratio is increased, by a factor of approximately $N^{0.5}$, if N is the number of outputs (Båth, 1979).
3. The array of stations may yield more information about the nature of the signals (e.g the apparent velocity of the seismic signals along the profile line).

4. DATA PROCESSING

4.1 Comments on Raw Data

The refraction data for the present study consist of six profiles. Since we are interested in only the regional structure, no corrections were applied for shot size, receiver elevation, and water depth for this preliminary interpretation. Owing to equipment malfunctions, 5 records from the U. of A. digital array were found to be unusable, and were edited out; the amplitudes of twelve records from various recording systems were also incorrect up to an order of magnitude (Ellis and Clowes, 1981, p.23). Because of this, we normalized each trace to a maximum amplitude of unity for plotting purposes. Furthermore, when the shots were detonated, all receiver channels were not turned on at the same time. As a result, the WWVB time is needed for each receiver channel to align them correctly with respect to the shot instant.

In general, some of the features present in the raw refraction data are:

1. The amplitudes of the nearest seismic trace are significantly larger than the most distance ones.
2. Beyond 150 km from the shot, the amplitudes of first arrivals become small and not distinct from the noise background.
3. Because of high noise levels at large distances and a

small amplitude of Pn, only the profile F1 shows the first arrivals which may be identified as a Pn phase.

4. A discontinuity in the travel-time curve is observed on profile F1 at a distance of about 210 km from the shot point, but the discontinuity of the reversed profile N2 is not observed because of the high noise levels.

4.2 Spectral Analysis

A seismic trace is a time representation of ground motion following the explosion of the source. The application of the Fourier transform converts the time-domain measurements of the seismic trace into frequency domain measurements, thus the amplitude for each frequency component can be evaluated through the Fourier transformation. A power spectrum is a measure of the square of the amplitude for each frequency. Knowledge of frequency, amplitude, and phase characteristics is extremely important in designing digital processing techniques to improve seismic data. Båth (1974) provided a comprehensive summary of theory and applications of spectral analysis in various geophysical desciplines.

The finite length of seismic data represents the truncation of the infinite data by a rectangular function. The discontinuity between the beginning and the end of data creates undesirable side-lobe effects in the frequency domain, thus the power spectrum of the truncated data may be

negative at some frequencies. A Daniel window, which represents the closest inverse of a rectangular window in the frequency domain, is useful to apply on data to eliminate the undesirable effect of the truncated data and to reduce the variance of the power estimate. Kanasewich (1975, p.96-105) presented a detailed discussion of the theory and the computational procedure of Daniel power estimate and he recommended the use of the Daniel spectral estimate when the data set had 100 to 4000 samples.

In the time domain (or lag domain if we calculate the power spectra with the autocovariance function) the Daniel window is defined as :

$$W(k)=\sin(ak/m)/(ak/m) \qquad k=0,1,2,....n-1$$

where:

a = 3.1416,

n = the number of observations,

m = the width of the window.

The parameter m controls the resolution of the spectral estimate; the greater the value of m, the greater will be the resolution. However, the greater the value of m, the greater will be the variance of the spectral estimate for a given value of n. Usually m is chosen to be about 10 to 20 % of n.

A computer program written by Robinson and Siliva(1979) was used to compute the Daniel power spectrum in this study. The program first computes the autocorrelation of the data,

weights the autocorrelation values by the Daniel window, and then collapses all values like an accordian to length m (the width of the window). The Fourier transform converts the collapsed autocorrelation values into the frequency domain, thus the power spectrum is estimated at equi-spaced frequencies between zero and the Nyquist frequency.

Fig.4.1 to 4.3 show the power spectral estimates at various locations of increasing distances from the shot A1. These figures indicate that the high frequency components of the seismic signals decrease as the distance increases. This implies that the high frequency components are filtered out by the earth as the seismic waves travel greater distances. In Fig. 4.1 to 4.3 it may be observed that the upper limit of significant power decreases from about 20 Hz at a distance of 25 km to about 11 Hz at 152 km. On the whole, the frequency content of 'useful' signal energy is restricted to a range of 5 to 20 Hz. A bandpass filter of 5-20 Hz was applied to records from profiles A1, A2, N1, and F2. However, for the profile F1 and N2, where the distances between the shots and the recording stations were over 100 km, the records were filtered with a bandpass of 2 to 10 Hz.

Fig.4.4 and 4.5 show the dramatic [illegible]nce of frequency contents in marine shots from th[illegible] N1 and F2. The two shots were located at the [illegible] a water layer with depths of 60 and 110 m respec[illegible]ly. The power spectra exhibit the anomaly of water-layer reverberation: the reverberation of the signal between the top and bottom

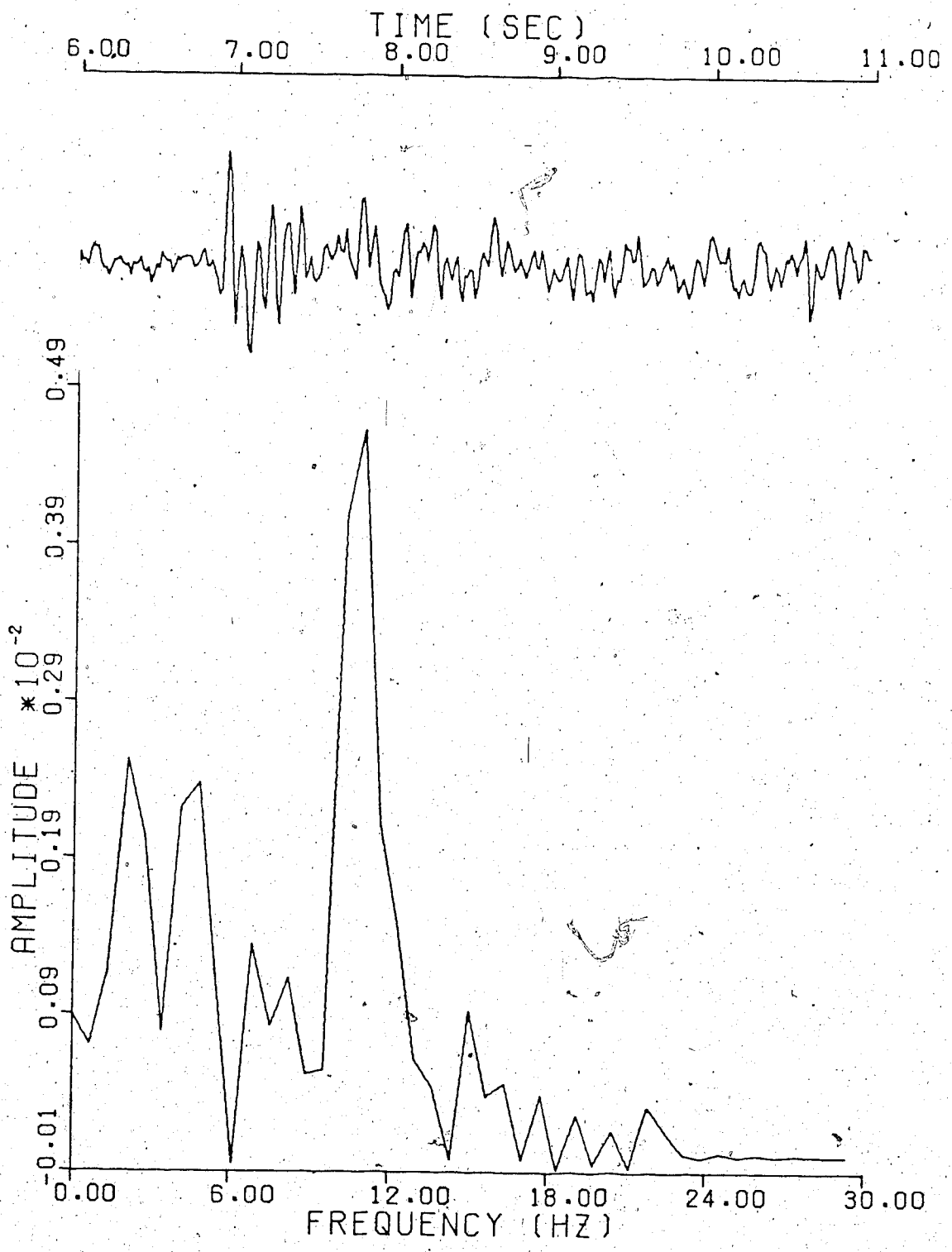

Figure 4.1 The power spectrum for refraction line A1. The distance is 24.6 km from the shot.

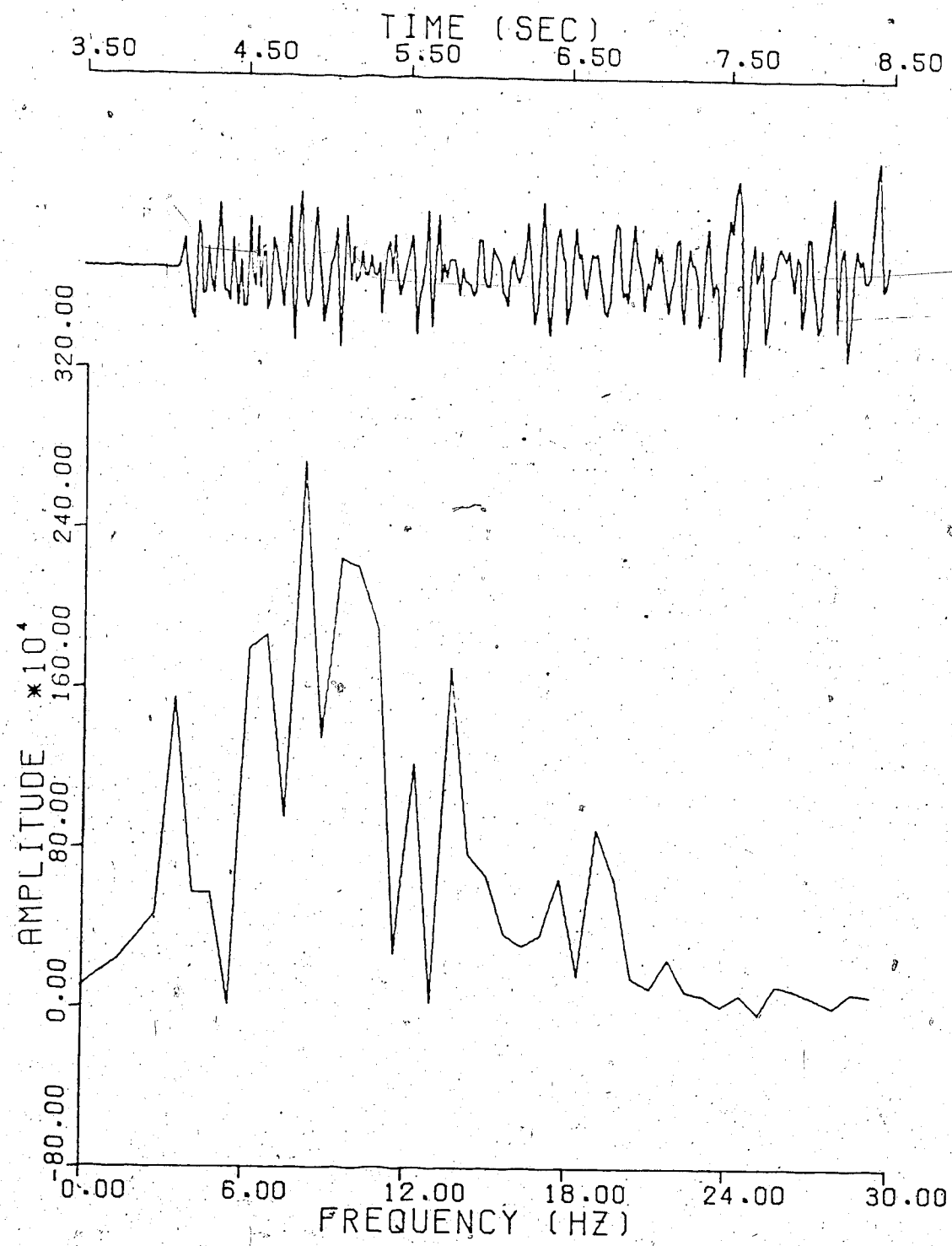

Figure 4.2 The power spectrum for refraction line A1. The distance is 41.2 km from the shot.

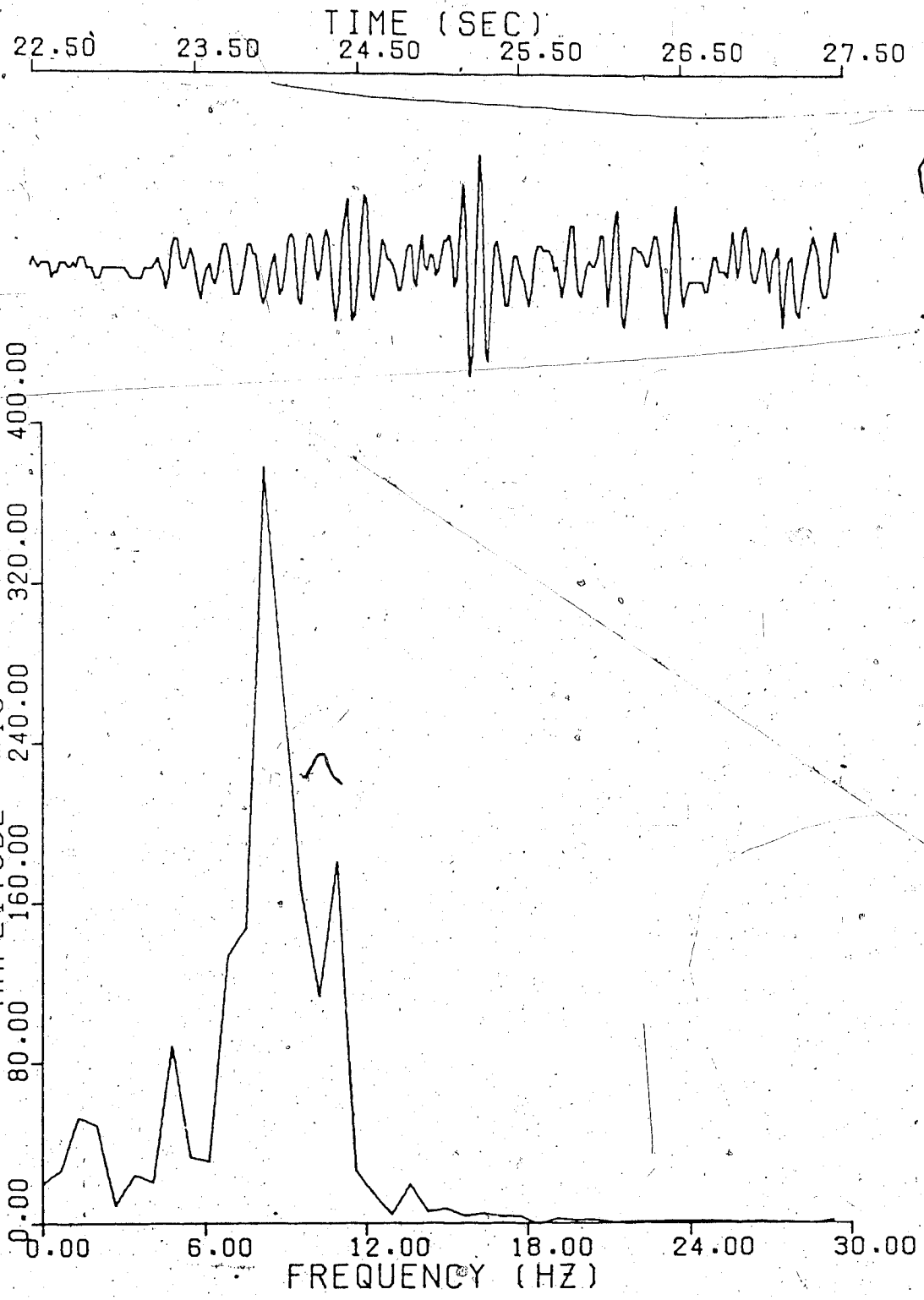

Figure 4.3 The power spectrum for refraction line A1. The distance is 152.0 km from the shot.

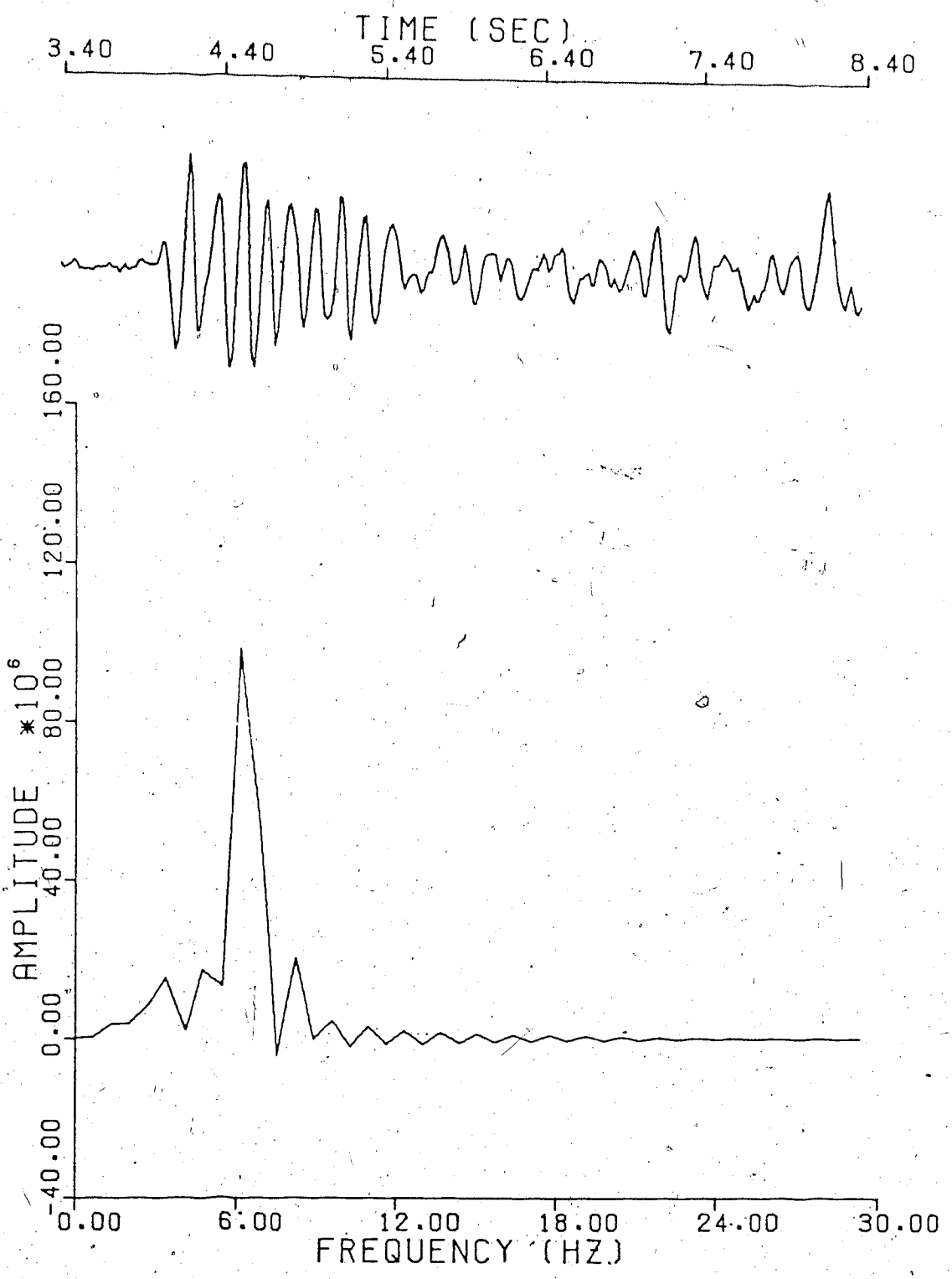

Figure 4.4 The power spectrum of marine shooting for line N1. Note the large amplitude at 6.0 Hz due to water reverberation.

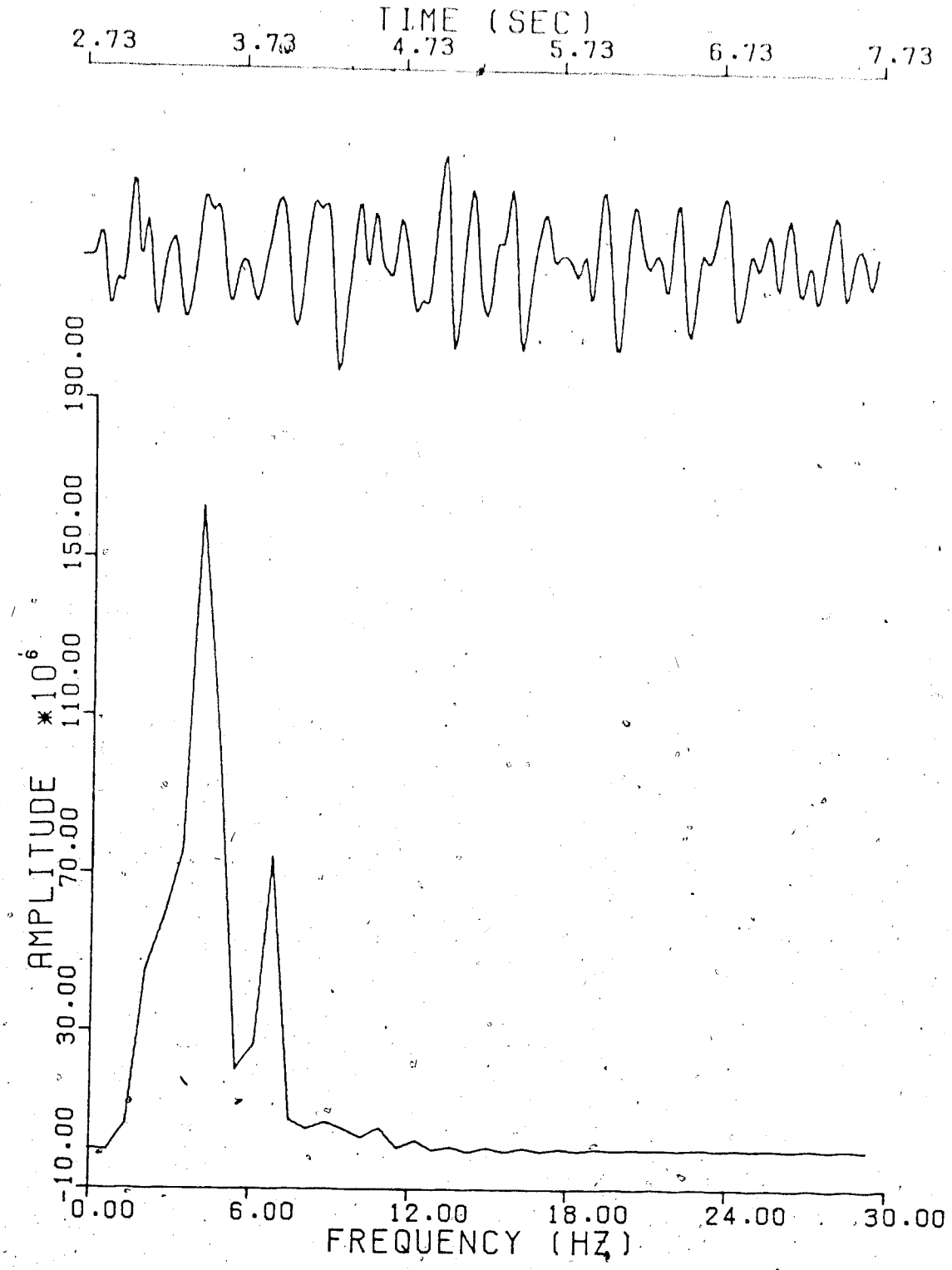

Figure 4.5 The power spectrum of marine shooting for line F2. Note the large amplitude at 3.7 Hz due to water reverberation.

of the water layer gives rise to a sharply defined maximum in the frequency response. The two peak frequencies are at 3.7 and 6.0 Hz respectively. The application of deconvolution filters is often suggested as a mean of removing reverberation effects which obscure the recorded signals. These filters might be useful for some of the present data, particularly when the later arrivals are to be studied.

On the other hand, the power spectrum of the water reverberation is useful to estimate the depth of the water layer. The relation between the peak frequency and the water depth is expressed (Dobrin, 1976) by

$$f=v/4d$$

where:

f = peak frequency,

v = velocity of sound in water,

d = water depth.

Two examples are used to illustrate that the water depth can be estimated by the power spectrum of water reverberation using the above formula. Table 1 summarizes the results of the measured water depths (d_1) (Ellis and Clowes, 1981, p.12) and water depths (d_2) determined from the power spectra.

Comparison of the measured water depths and depths by power spectra from the two seismic records (Table 1) shows only minor differences. This indicates that the depth of the water layer can be estimated from the power spectrum of data

geophone	v(m/s)	f(Hz)	d_1 (m)	d_2 (m)
60021	1490	6.0	60	62
450041	1490	3.7	110	100

Table 1.... Comparison of the results of the measured water depths to the depths determined from power spectra.

which contain the signals of water reverberation.

4.3 Bandpass Filtering

A bandpass filter is a frequency filter designed to pass signal frequencies in a particular band and to attenuate all other frequencies. The purpose of applying a bandpass filter to seismic signals is to extract useful signals from noise background. The operation of filtering is especially effective in cases where signal and noise spectra do not overlap over a wide frequency band. Two types of bandpass filters are considered in this study: eight-pole, zero-phase shift, recursive Butterworth and Bessel bandpass filters. The effectiveness of both filters is compared on the data containing the first arrival of energy, and noisy data.

Kanasewich (1975, p.175-203) provided a detailed discussion of the 8-pole Butterworth filter. By specifying the attenuation rate at a high and low cutoff frequencies,

the filter coefficients are evaluated from poles and zeros of the Butterworth polynomial in a Z-plane representation. The input data are then convolved with filter coefficients recursively in both forward and backward directions to achieve zero phase shift filtering.

The design of a 8-pole Bessel filter is based on the Bessel polynominal. The derivation of filter coefficients is carried out in a similar manner to those for the Butterworth filter. A good discussion of the Bessel filter is given by Lubkin (1970).

Comparison of the Bessel and Butterworth filters shows the following differences:

1. The Butterworth filter has a much faster transition region from passband to stopband, and has a much better amplitude characteristic than that of the Bessel filter.
2. In the time domain, the Bessel filter has a only a tenth the overshoot of the Butterworth for filters up to five poles, and gets better as more poles are added, while the Butterworth filter gets worse.

Both filters were applied to the data that contained the first arrival of energy. Fig. 4.6 to 4.8 show the application of both filters on the first arrival over various frequency bands. The Bessel filter has little distortion on the first arrival in a range of frequency bands, but the Butterworth filter introduces a significant offset on the first arrival, as the frequency band gets narrower. For example, at the frequency band 5-12 Hz, the

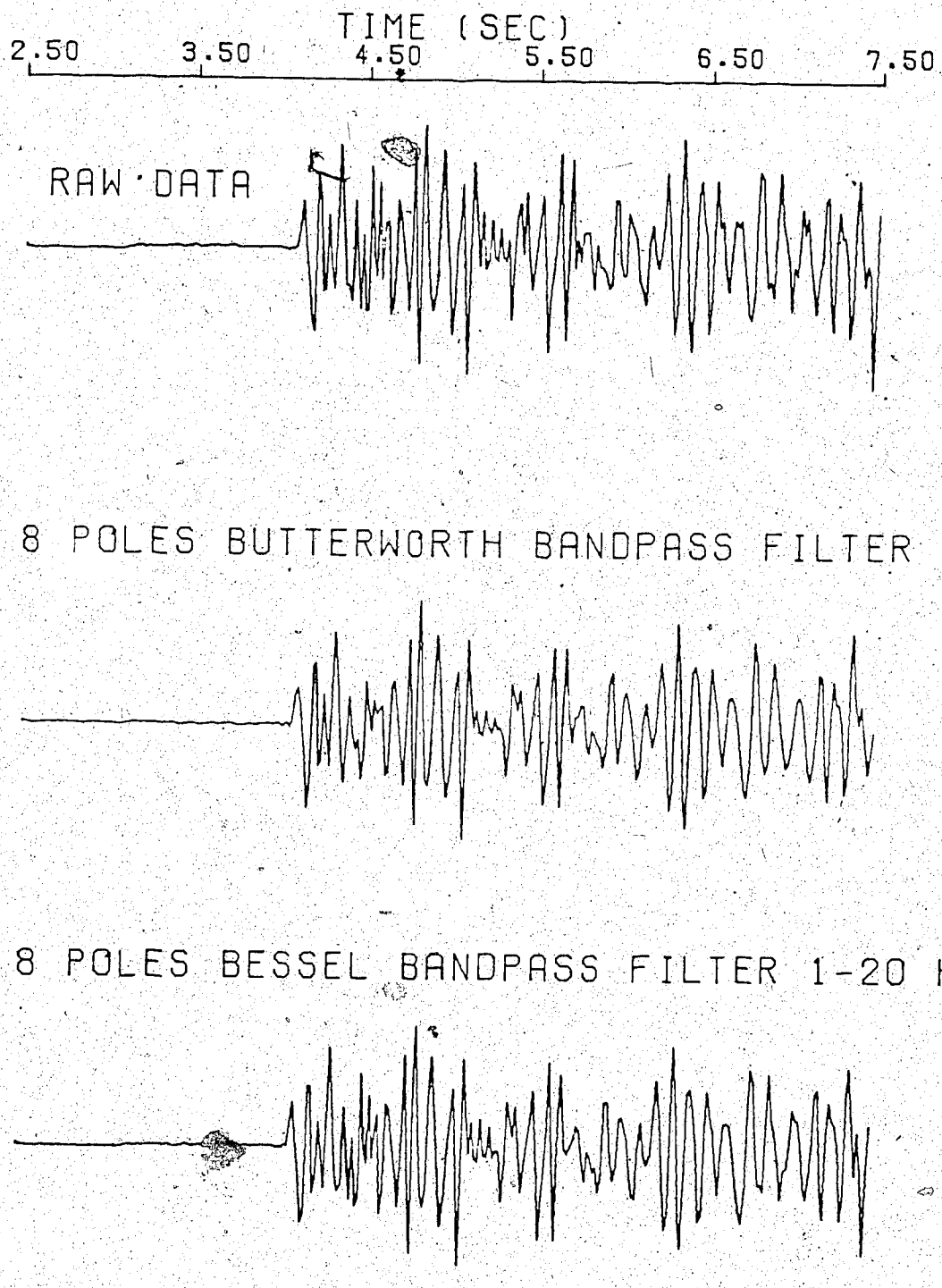

Figure 4.6 Comparison of Butterworth and Bessel bandpass filters on the first arrival in the frequency band of 1-20 Hz.

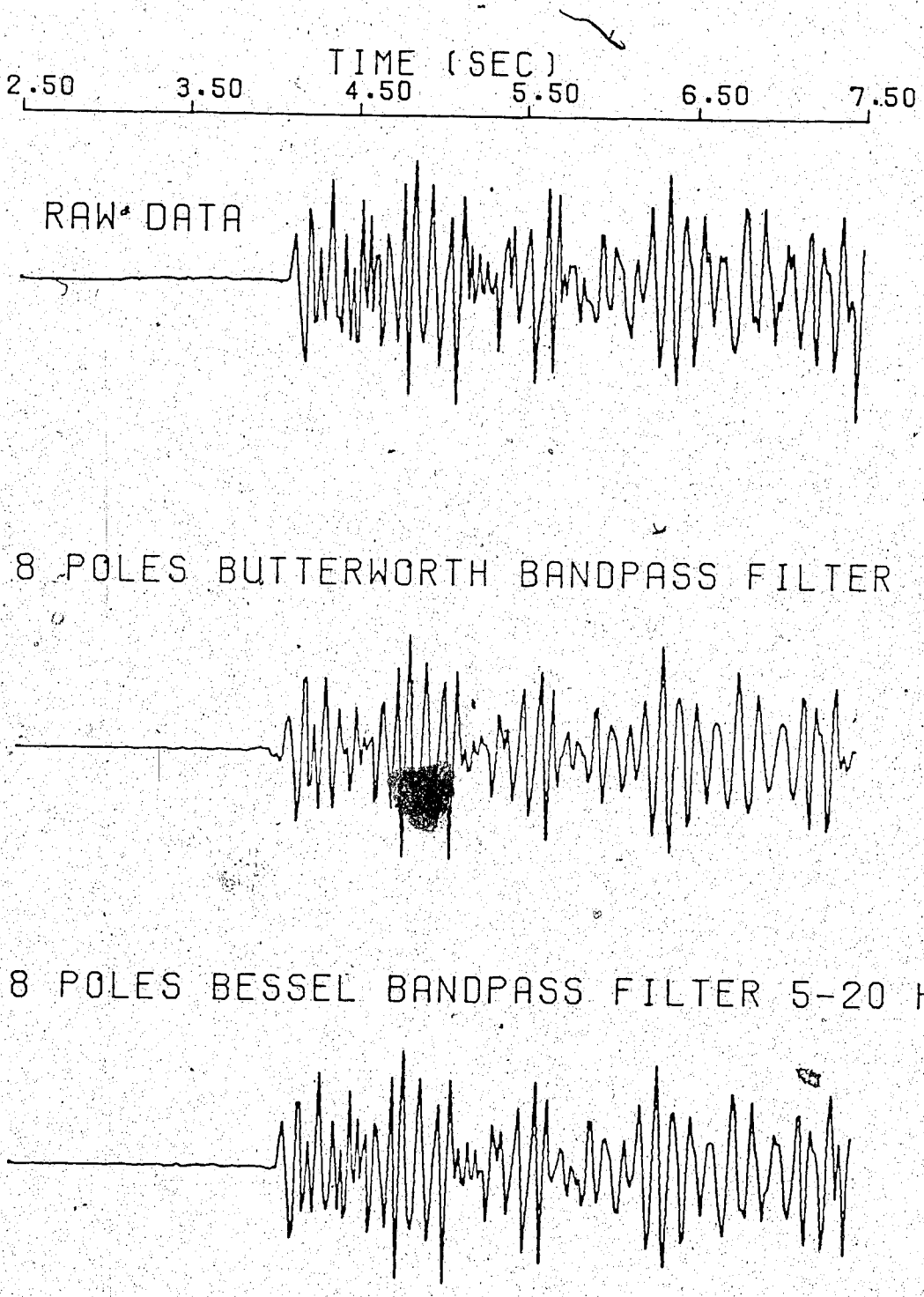

Figure 4.7 Comparison of Butterworth and Bessel bandpass filters on the first arrival in the frequency band of 5-20 Hz.

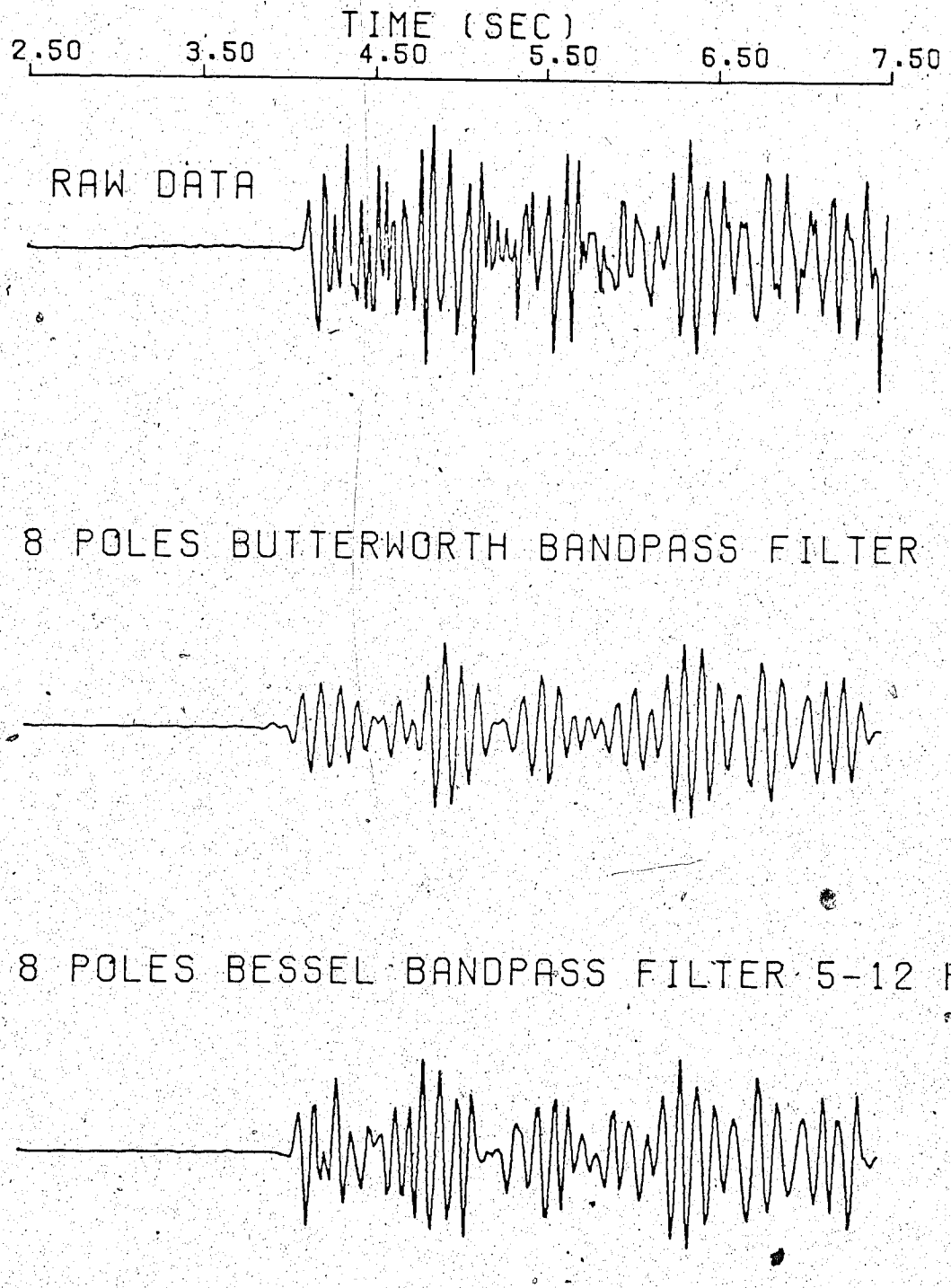

Figure 4.8 Comparison of Butterworth and Bessel bandpass filters on the first arrival in the frequency band of 5-12 Hz.

Butterworth filter offsets the first arrival time by 0.2 sec. This indicates that the Bessel filter is more suitable to apply on the data that contains first arrival energy, for the Bessel has a rather smooth transition region from the passband to stopband and tapers off the input data more gradually, thus avoiding distortion of the signals.

Both filters were then tested on a noisy record. Fig. 4.9 and 4.10 display the raw data and the data filtered by both filters. Comparison of the two filtered records shows the following features:

1. The Butterworth filter clearly suppresses the undesirable high and low frequency noise outside the passband.
2. The Bessel filter is not able to suppress completely both high and low frequency noise outside the passband. For example, the low frequency noise about 1.3 Hz (trace 3) is still present in the record.
3. Both filtered records have improved the correlation of seismic traces considerably.
4. The appearances of both filtered records are very similar to each other.

The Butterworth filter, in general, has better performance than that of the Bessel filter in extracting signals from noise background. The rapid transition from passband to stopband of the Butterworth is quite good to obtain a specific band of frequencies, and efficient to attenuate other frequencies that are outside the passband.

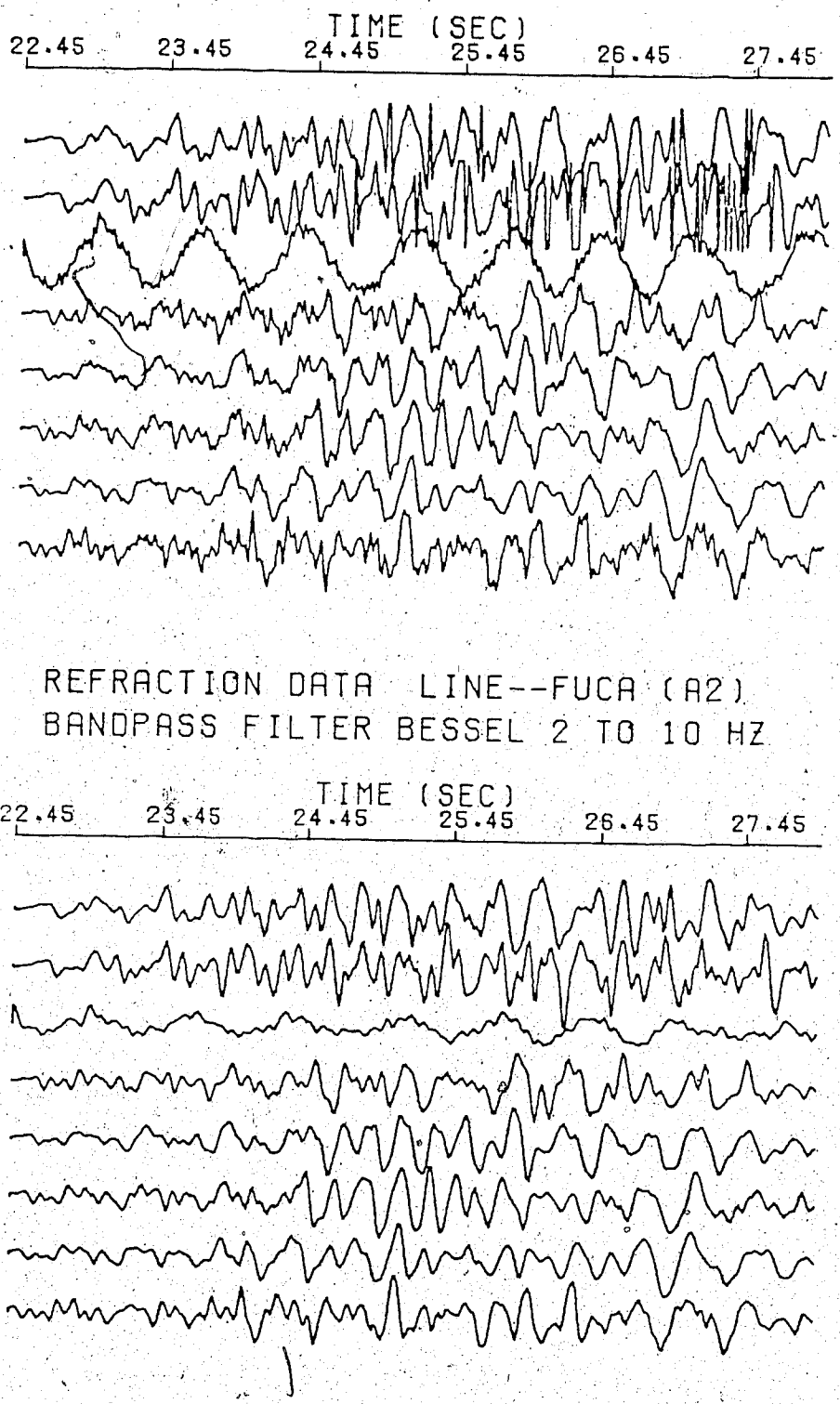

Figure 4.9 The raw refraction record and the corresponding record filtered by a Bessel bandpass filter.

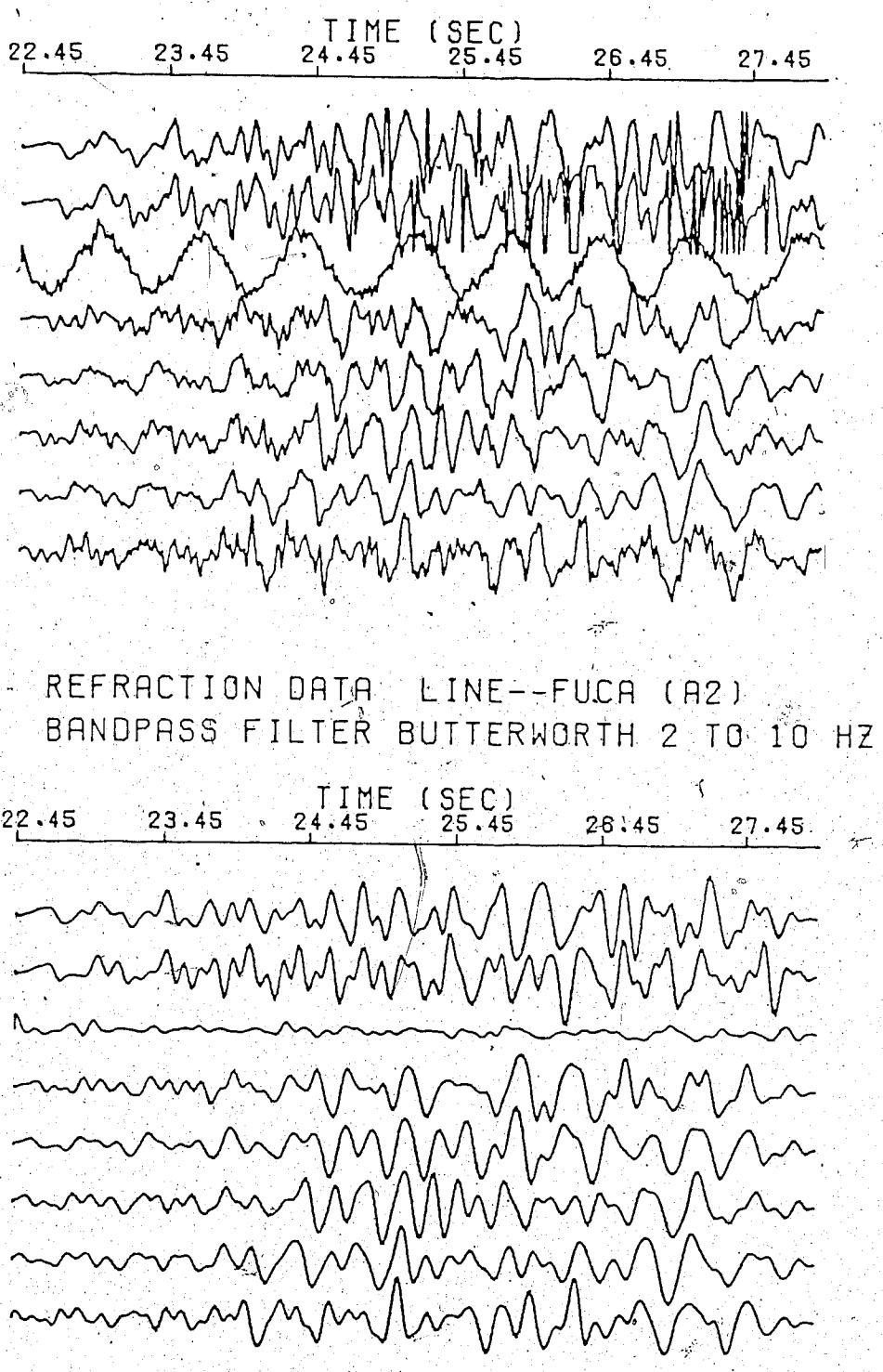

Figure 4.10 The raw refraction record and the corresponding record filtered by a Butterworth bandpass filter.

However, since the travel times of first arrivals are our main interest, the minimum distortion on the first arrivals introduced by the Bessel filter is more desirable. Thus we decided that the Bessel filter would be used on all seismic records.

It should be noted that in the form in which the Bessel filter was used in this work, the effective bandpass is considerably wider than that of the Butterworth filter with the same specified frequencies. Thus the poorer low frequency rejection of the Bessel filter is a function of larger bandwidth and could be improved by narrowing the nominal bandwidth.

5. VELOCITY-DEPTH DETERMINATION FROM REFRACTION DATA

5.1 Comments on Refracted Waves from the Crust

Since attenuation and absorption of elastic waves through the earth cause the amplitudes of elastic waves to decrease with increasing distance, study of the amplitude is essential to understand how the head wave propagates through the earth. Grant and West (1965, p.181) summarized three important facts for the propagation of head waves through the earth: 1. the head-wave amplitude diminishes inversely as the square of the distance from the source; 2. since the absorption coefficient is directly proportional to frequency, the head-wave amplitude also diminishes with frequency with the increase of travel time; 3. the energy in the head wave becomes maximum at the critical distance (the point where the refracted wave meets the reflected wavefront).

Based on travel-time analysis, three dominant seismic waves are observed from the surface down to the upper mantle:

1. Pg is usually assigned to be a refracted wave in the upper crust, which has a typical velocity of 5.5 to 6.1 km/s. The Pg phase is usually observed up to a distance of 60-100 km. In general, the amplitude of the Pg phase decays inversely as the square of the distance from the source; beyond 100 km its amplitude becomes very small,

and sometimes is not even observable.

2. The next prominent phase, which travels in the lower crust, is designated as P^*. However, this prominent phase is only observed in some regions (Berry, 1973). The absence of P^* phase is probably due to lateral heterogeneities in lower crustal layer. The typical velocity is between 6.8 to 7.1 km/s.
3. Pn is generally considered to be a head wave which travels directly beneath the Moho discontinuity. In general, the Pn phase is observed to be a first arrival at distances beyond 120-200 km. Because of the attenuation and absorption of elastic waves through the earth the amplitude of Pn decays rapidly beyond the critical distance. The typical Pn phase velocity in British Columbia is between 7.8 to 8.1 km/s.

5.2 Record Representation

All seismic sections were represented on a reduced travel-time diagram, where

$$T = t - D/V$$

with:

T = reduced travel time,

t = travel time of seismic arrivals,

D = source-receiver distance,

V = reduction velocity.

This kind of display of data gives much better resolution on a given graph when large recording distances are involved, since, when the reduction velocity is close to the phase velocity of particular events of interest, these are more or less horizontal on the diagram. This reduced-time representation offers the advantage of representing more time data within a given graph, or conversely allowing an expanded time scale to be used. Since the Moho discontinuity was of a particular interest in this study, a reduction velocity of 8.0 km/s was applied on all record sections.

5.3 Correlation of Refraction Arrivals

Correlation of first arrivals from trace to trace is essential to determine the apparent phase velocity of a particular travel-time branch in the refraction interpretation. In general, the attenuation and absorption of elastic waves in rock cause a progressive lowering of apparent frequency of seismic events with increasing distance of travel through the earth, thus the shape of the waveform changes as a function of distance. In addition, when noise is present in some records, it is difficult to observe the exact instant of onset of the first break energy. Thus, it is common practice not to use the beginning of the event for correlation purposes, but the pronounced maximum or minimum amplitude following the first arrivals of

energy. The correlation of convenient peaks or troughs of the seismic signals which have similar appearances provides a more reliable estimate of apparent velocity of the travel-time branch. In order to determine the actual arrival times, we need to make a phase correction from the picked value of the peak or trough, back to the estimated beginning of the refraction pulse.

5.4 Plane-Layered Interpretation

First arrivals were picked from all record sections, except the last two-thirds of the first arrivals on profile N2. Linear segments of travel times were fitted in a least-square program to determine velocities and intercept times of the refraction waves that travel at different depths. The determination of the near surface velocity was not well defined due to the relatively large separation of recording sites. The travel time to the first recording site from four shot locations yields a range of near surface velocities from 14.1 km/s to 4.57 km/s (Table 2). The one extremely high apparent near surface velocity (14.1 km/s) is definitely due to an error of the start time, therefore, it is reasonable to ignore this high surface velocity. The velocity from the shot A1 and F2 are close to an average velocity of 5.3 km/s. This average velocity is considered to be an upper limit of near surface velocity and can be used to compute the necessary models for the preliminary

refraction line	geophone station	distance km	time sec	surface velocity km/s
A1	450011	3.308	0.626	5.28
A2	10051	3.671	0.803	4.57
F2	450041	14.743	2.766	5.33
N1	10021	2.036	0.144	14.11

Table 2.... Near surface velocities from seismic profiles of A1, A2, F2, and N1.

refraction interpretation.

The depth to the refractor was calculated from the intercept time using a horizontal plane-layered model. A computer program listed in the Appendix allows the calculation of the models for n-horizontal layers.

Central Profiles

Fig.5.1 shows the Argo refraction profile (A1). This profile consists of a near surface layer and two distinct deeper layers. The velocities of these layers are 6.35 and 7.02 km/s. The corresponding thicknesses are 0.51 km for the surface layer and 10.5 km for the upper crust. The noise levels in this section are not significant; the first arrivals have relatively large amplitudes and correlate very well throughout the whole section.

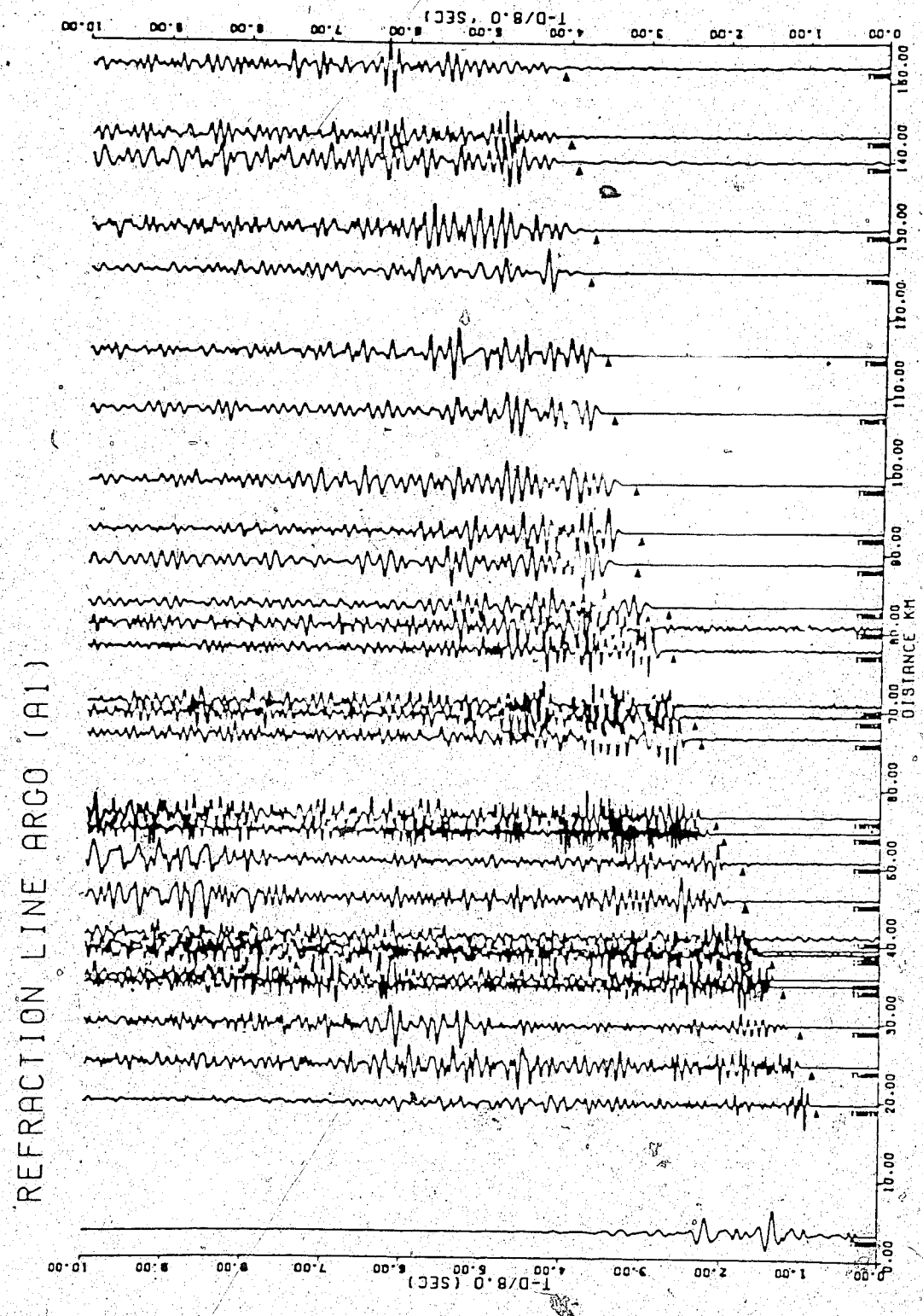

Figure 5.1 Vertical component reduced section of line A1. Small ticks on traces indicate first arrival picks.

Fig.5.2 displays the record section of profile A2. This section is similar to section A1. The first arrivals from both lower and upper crust are clear and well defined. Their velocities are 6.39 and 6.99 km/s, corresponding to thicknesses of 0.58 and 13.1 km respectively. Comparison of crustal velocities with profile A1 shows that both velocities are in excellent agreement, but the thickness of the upper crust has a rather large discrepancy between two profiles. This discrepancy is up to 2.6 km. This implies that the crustal structure beneath the shot A is not a simple horizontal model, and that lateral variations of structure may be present.

Nero Profiles

Fig.5.3 and 5.4 are profiles of the observations from the northern end along the structural axis of Vancouver Island to the southern end of the island. Fig. 5.3 is the reversed profile of Fig. 5.1. The first arrivals are clear and coherent up to a distance of 210 km from the shot. The data were well fitted into two linear segments which correspond to the velocities, 6.57 and 7.04 km/s respectively. The very high noise levels and small amplitudes of refracted first arrivals made the correlation beyond 210 km very difficult. A narrow bandpass (2 Hz to 5 Hz) was applied to the data in attempt to recover signals from the noisy background, but the low signal-to-noise ratio made travel-time picks ambiguous so that the determination

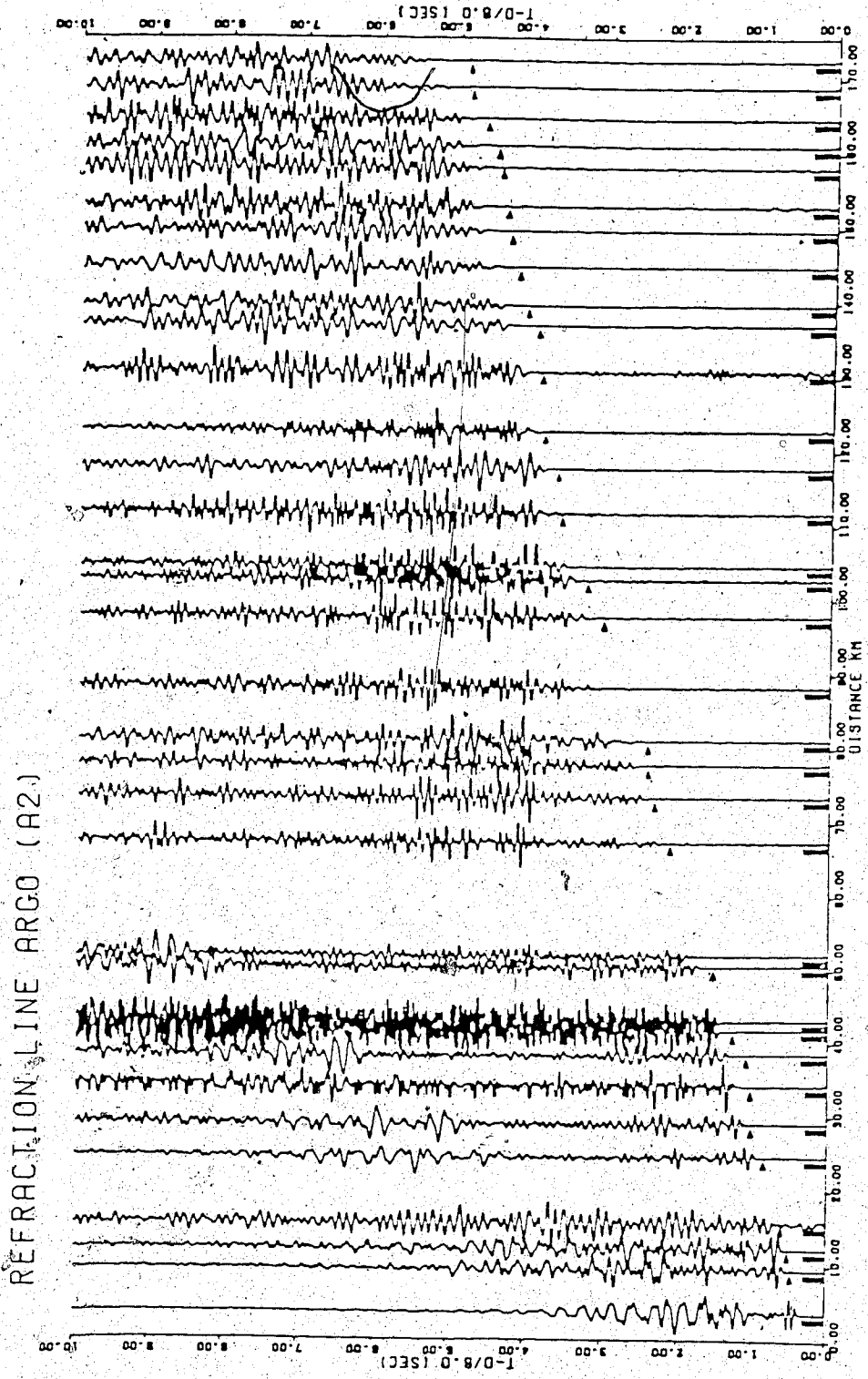

Figure 5.2 Vertical component reduced section of line A2. Small ticks on traces indicate first arrival picks.

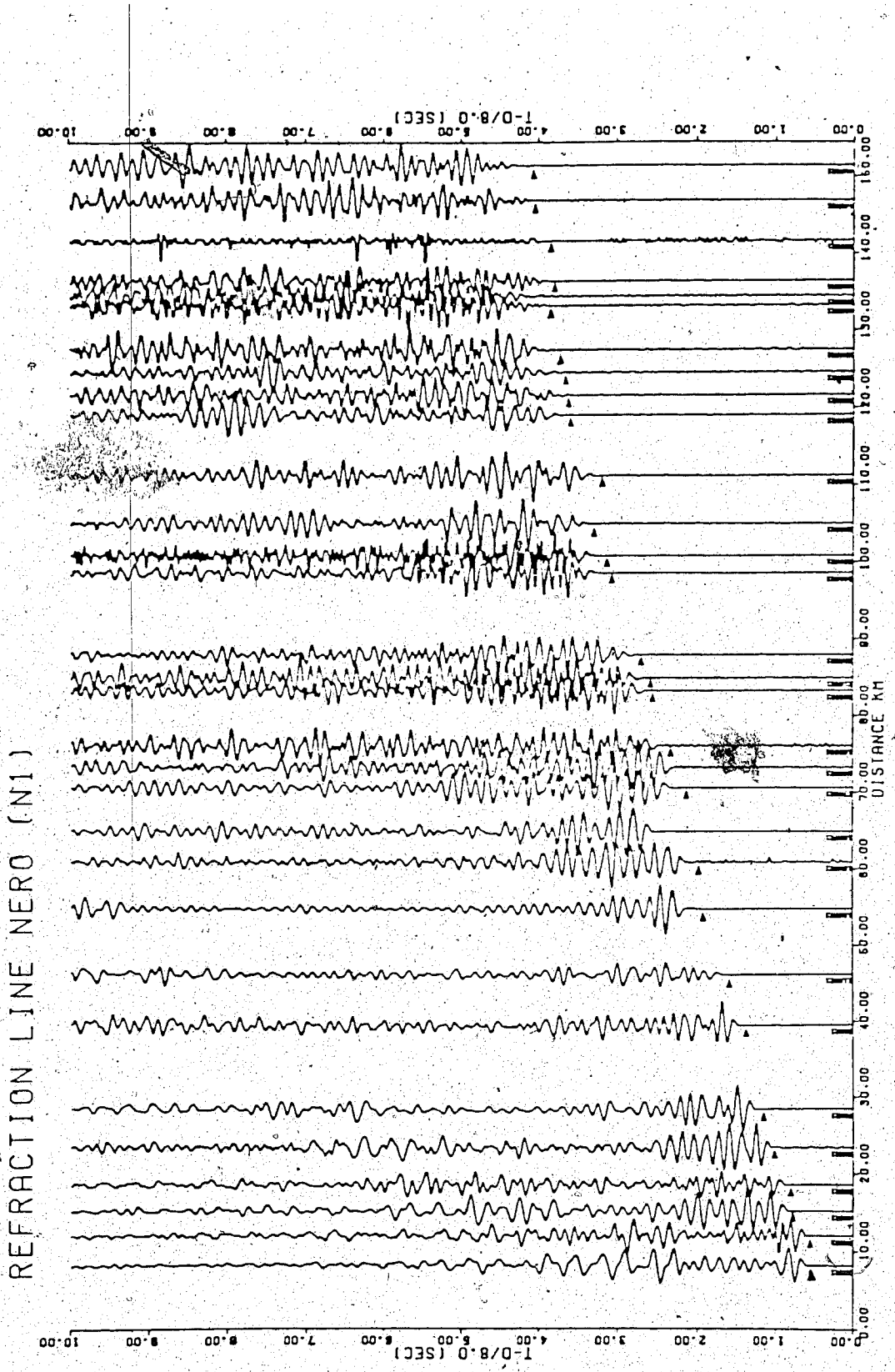

Figure 5.3 Vertical component reduced section of line N1. Small ticks on traces indicate first arrival picks.

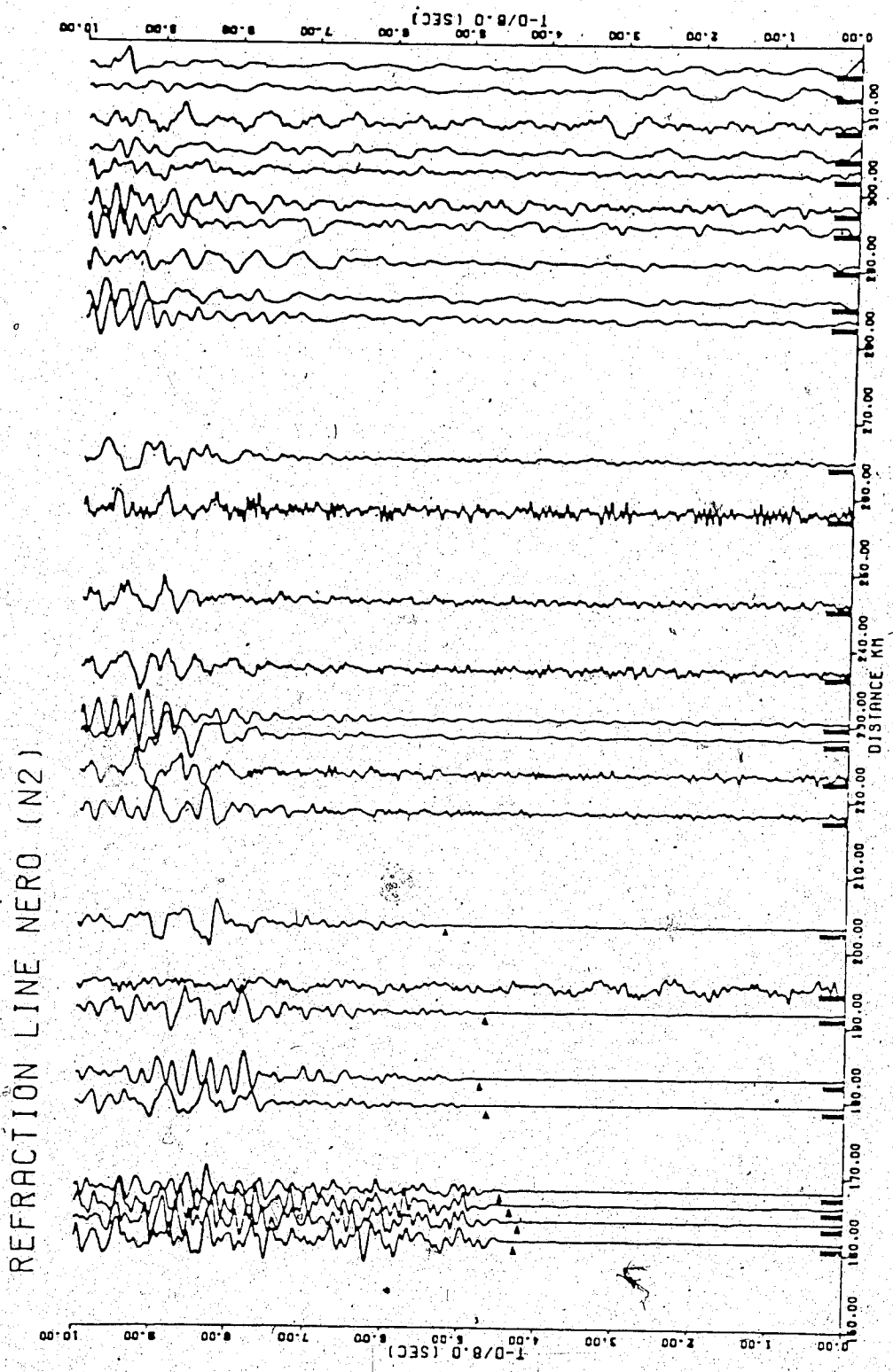

Figure 5.4 Vertical component reduced section of line N2.Small ticks on traces indicate first arrival picks.

of Pn phase velocity was not possible.

Fuca Profiles

Fig.5.5 and 5.6 represent the reversed section of the Nero profile. The profile F2 is similar to N1. The first arrivals of 6.52 km/s continues up to 100 km, but the arrivals from the lower crust are scattered. They were fitted approximately with a 6.95 km/s line segment. A discontinuity of travel-time curve is observed about 210 km from the shot on the profile F1. This discontinuity may indicate the existence of a low velocity zone. If such a low velocity zone exists in this region, it is difficult to establish the depth to the Moho from the refraction data. Arrivals identified as representing a Pn phase are observed on the profile F1 between the distance 220 to 290 km, but their amplitudes are quite small. In order to enhance the certainty of the Pn arrivals, we enlarged the amplitude of Pn arrivals and reduced the background noise considerably by applying a Butterworth filter with a bandpass of 1 to 2.5 Hz on the profile of F1. The Pn arrivals are clear and coherent in Fig.5.7. The apparent velocity was found to be 7.95 km/s. By assuming plane horizontal layers, the depth for the Moho determined from intercept times is 35 km (Fig. 5.6). Later arrivals in Fig. 5.7, which may be reflections from the Moho, appear fairly clear and coherent, with rather large amplitudes. Another feature noteworthy in Fig. 5.7 is the line C-C, postulated to be the secondary arrivals from a

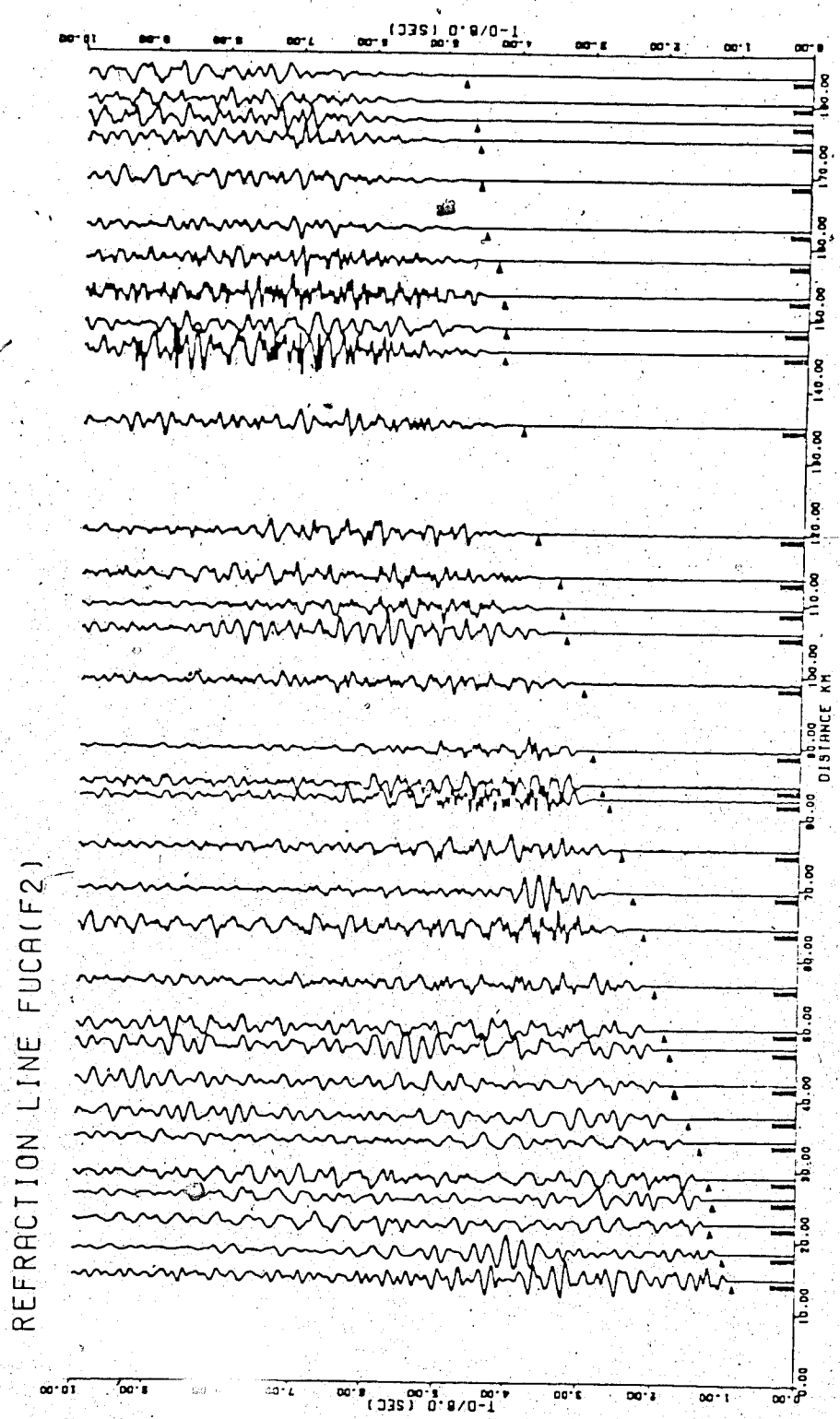

Figure 5.5 Vertical component reduced section of line F2. Small ticks on traces indicate first arrival picks.

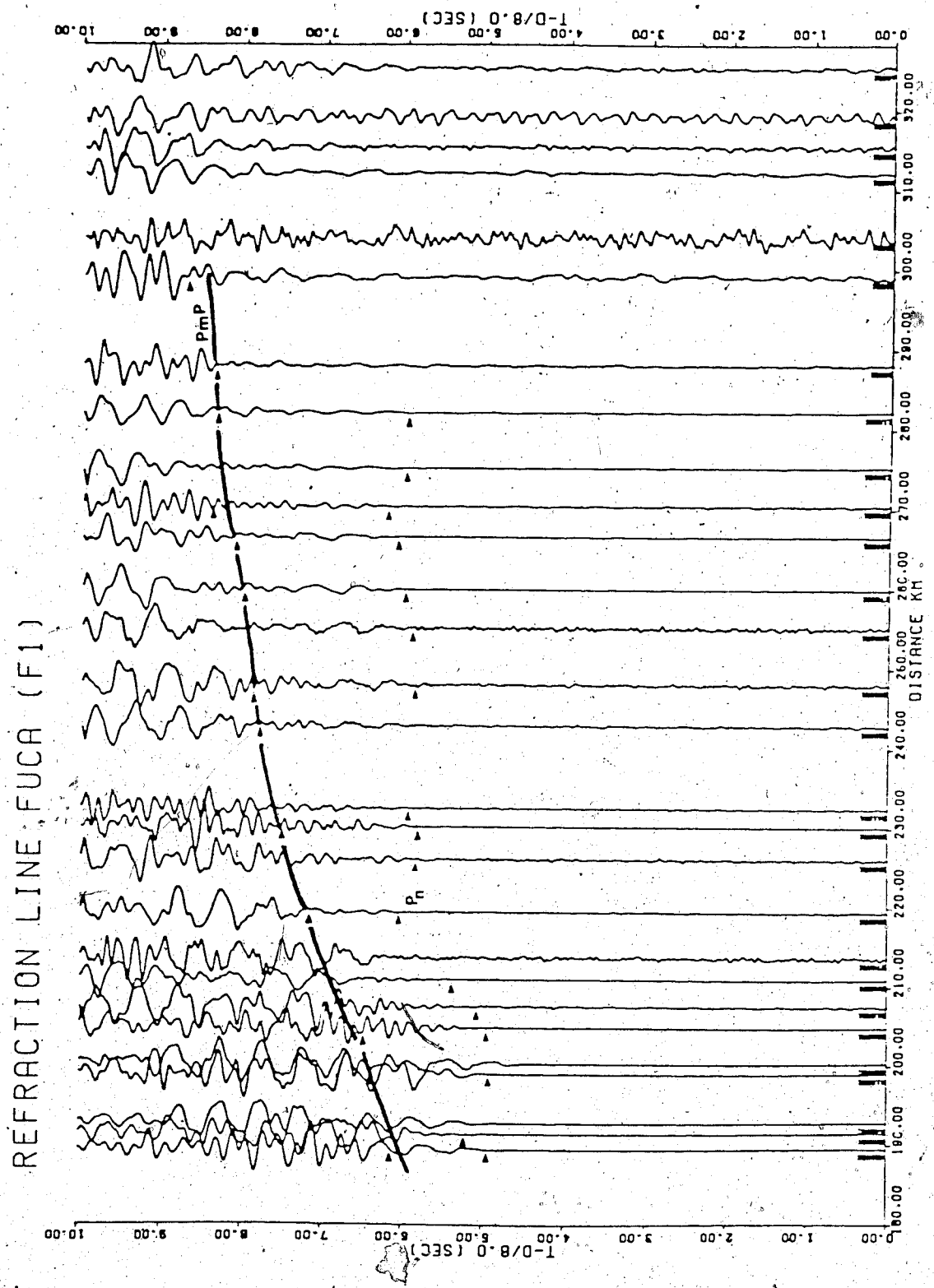

Figure 5.6 Vertical component reduced section of line F1. Small ticks on traces indicate first arrival picks. PmP=reflections from the Moho.

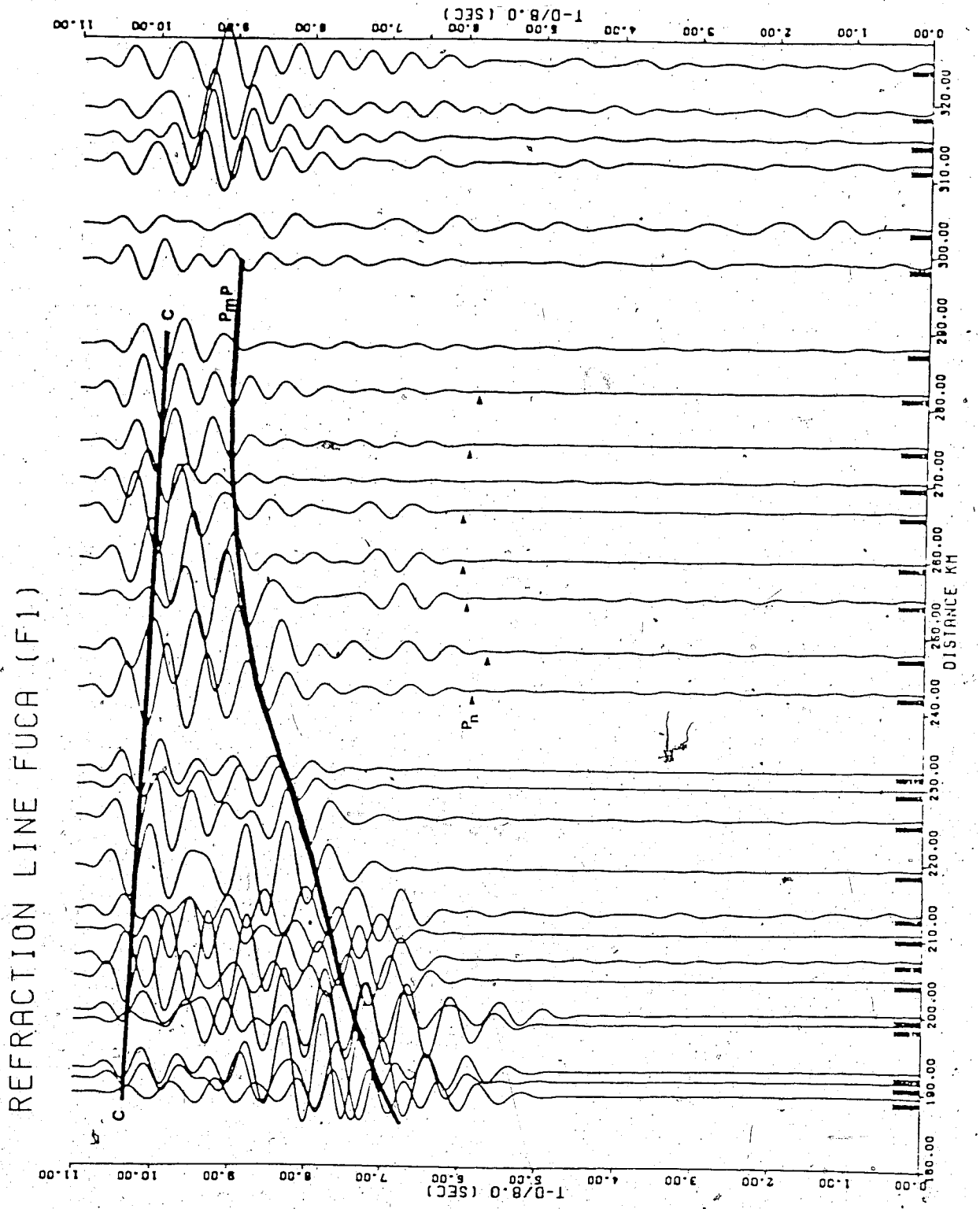

Figure 5.7 Vertical component reduced section of line F2. Small ticks on traces indicate first arrival picks. PmP=reflections from the Moho; CC=postulated secondary Pn arrivals from a sub-Moho refractor.

sub-Moho refractor. These secondary arrivals have fairly large amplitudes and an apparent velocity of about 8.3 km/s. Because of the truncation of the profile at 330 km, first break arrivals are not recorded for this later branch of Pn arrivals. Thus the interpretation of this later branch is not attempted.

5.5 Wiechert-Herglotz-Bateman (WHB) Inversion of the Travel-Time Curves

Although the simplified approach of a horizontal layer model provides useful information of an approximate velocity-depth function, it requires the calculation of thicknesses by a series of possible layers with a constant velocity for each layer. In reality, velocity usually increases with depth. Another approach, which makes use of velocity increasing continuously with depth, may represent a more realistic model of the earth. This approach is known as inversion of travel-time curve by WHB integral. Grant and West (1965, p.138-141) provided a detailed analysis of this approach.

We assume that the elastic waves travel through a succession of horizontal layers of different elastic media, and the velocity increases as a function of depth only. The WHB integral for plane horizontal layers may be shown to be:

$$Z(V) = \frac{1}{\pi} \int_0^D \cosh^{-1} \left(V \frac{dt}{dx}\right) dx$$

where :

D = the distance of a ray path that returns to the surface of the ground,

V = the velocity of the ray at the maximum depth of penetration,

dt/dx = the derivative of the time-distance curve.

Before the application of the integral, the travel-time data, excluding the data for the Pn arrivals, were reduced to the base of the surface layer by subtracting the times that were calculated from the intercept times of the plane-layered model. This removes the effect of the near surface layer. The travel-time data were then fitted by a polynomial of arbitrary degree. The use of the polynomial has certain advantages in analysing the data: 1. we can establish a concise mathematical formula to express the relation between two variables (in our case, time and distance); 2. although the degree of the polynomial to be fitted to the data may not be known in advance, we change the order of the polynomial until we reach an order for which we get a satisfactory result of fitting the data; 3. the polynomial is a continuous function and is differentiable anywhere within its domain, it is useful, for instance, for interpolation purposes or for smoothing the original data prior to further analysis.

In general, the degree of polynomial is not restricted. However, one condition is required in order to evaluate the WHB integral, that is: $V > dx/dt$. We found that the data of

sections A1, A2, and Nero fitted with a polynomial of second degree; the data of section Fuca, with the polynomial up to fourth degree. The coefficients of the polynomial, in turn, permit the evaluation of the WHB integral by determining the derivative of the time-distance curve at any arbitrary distance. A computer program listed in the Appendix was written for the inversion of the travel-time data by this method.

Fig.5.8 to 5.11 illustrate the application of the WHB integral to the time-distance curves of sections A1, A2, Nero, and Fuca. The velocity-depth functions of the four seismic sections are quite similar to a depth of 6 km; the velocity beneath the surface layer of 5.3 km/s gradually increases with depth from the initial velocity of about 6.2 km/s to a velocity 6.5 km/s at a depth of 6 km. Below this depth the velocity-depth curve of profiles A2 and Fuca have similar slopes, but their slopes are steeper than those from the profiles Nero and A1. As a result, the depth to any given velocity refractor from the profiles A2 and Fuca is greater than that from profiles Nero and A1. On the other hand, the velocity-depth curve of profile A1 has a minimum slope which, in turn, yields a minimum depth to a given velocity refractor. For example, the depth to a velocity of 7.0 km/s fluctuates from a maximum of 21.4 km from the profile A2 to a minimum of 16.5 km from the profile A1, with a intermediate value of 17.3 km from the profile Nero. This implies that the ray path travelled from A to F is quite

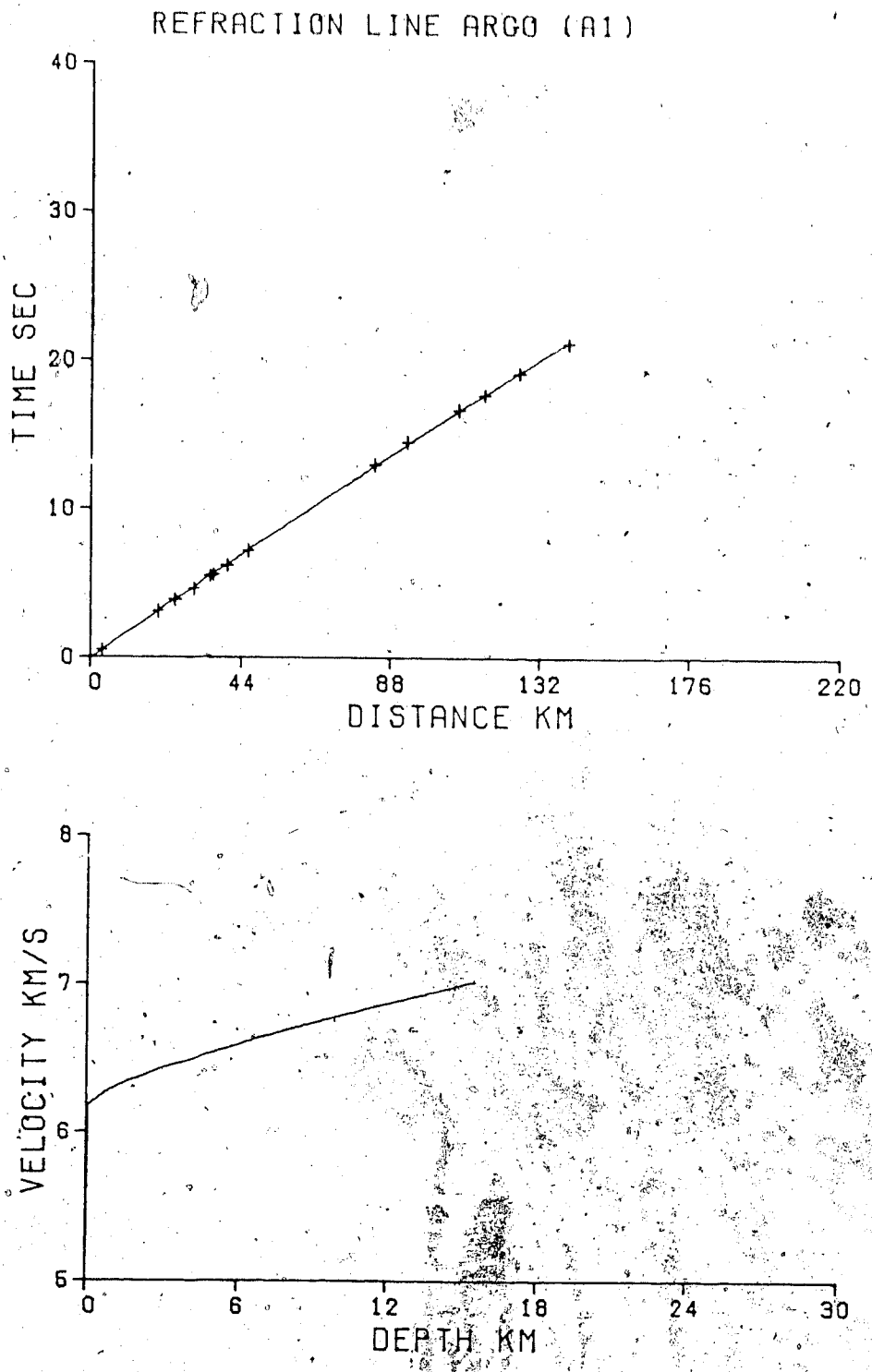

Figure 5.8 Time-distance curve: cross= raw data; solid line= data fitted by a polynomial, and the velocity-depth curve by the WHB inversion of time-distance curve beneath the surface layer.

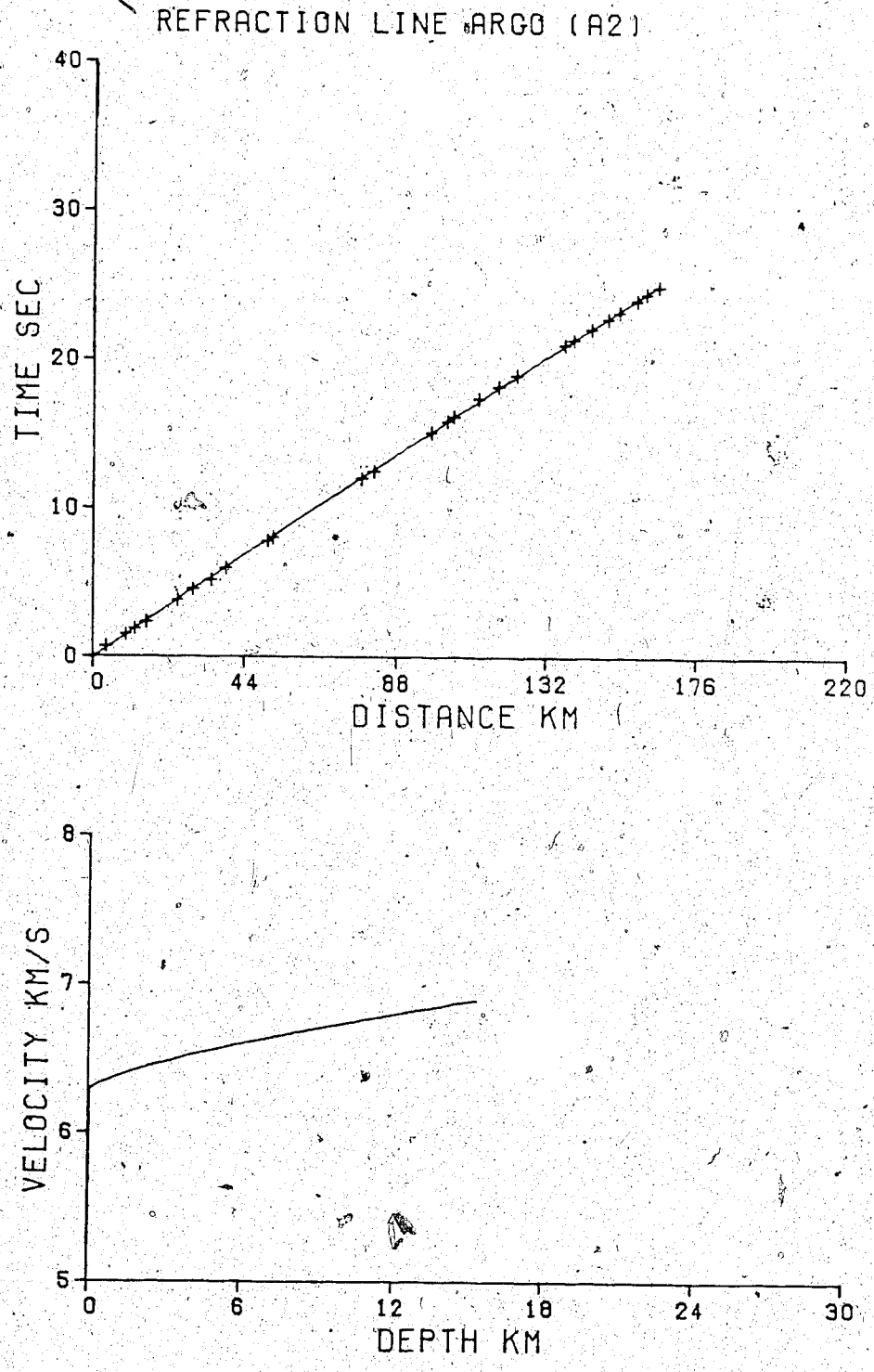

Figure 5.9 Time-distance curve: cross= raw data; solid line= data fitted by a polynomial, and the velocity-depth curve by the WHB inversion of time-distance curve beneath the surface layer.

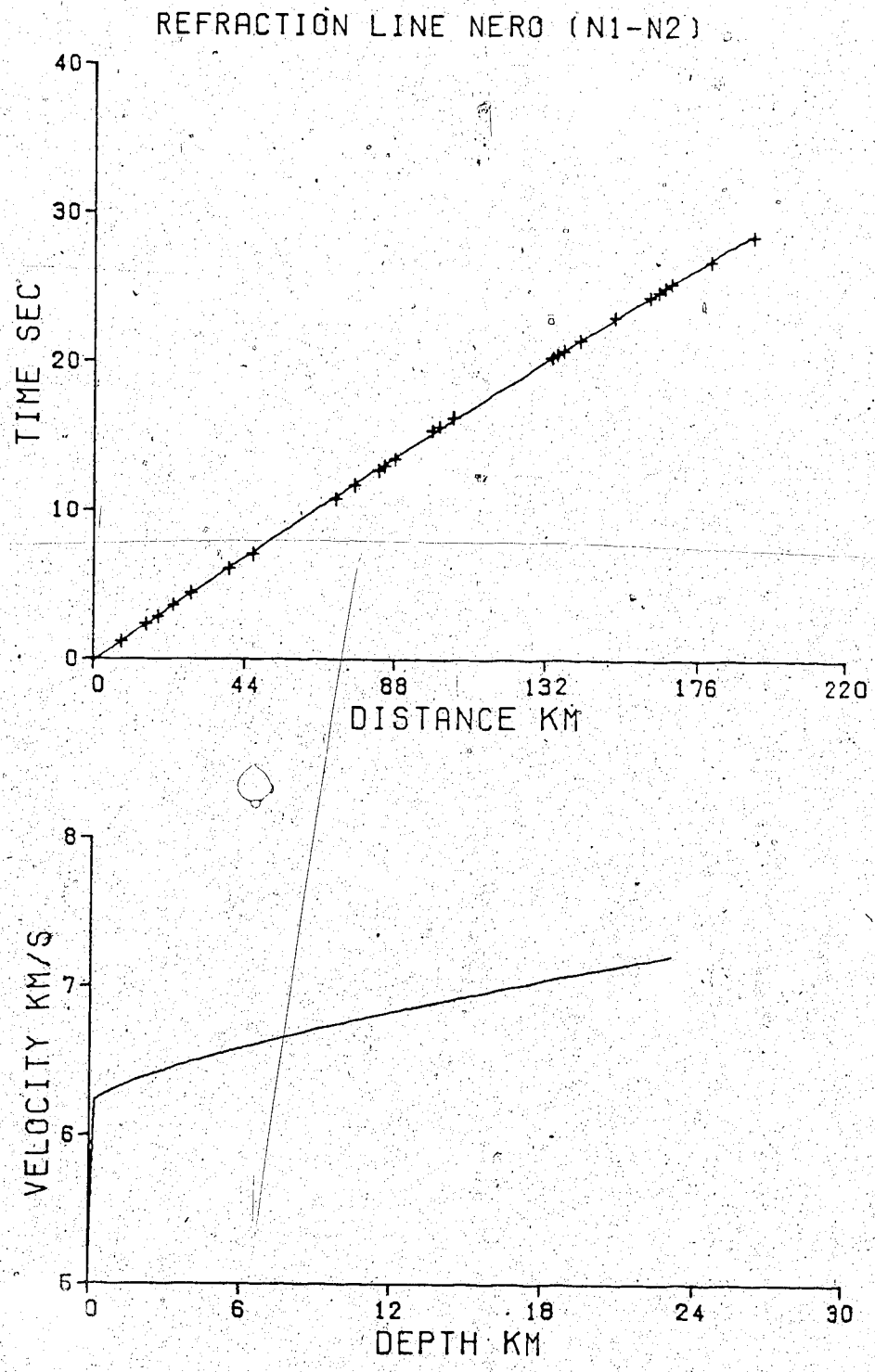

Figure 5.10 Time-distance curve: cross= raw data; solid line= data fitted by a polynomial, and the velocity-depth curve by the WHB inversion of time-distance curve beneath the surface layer.

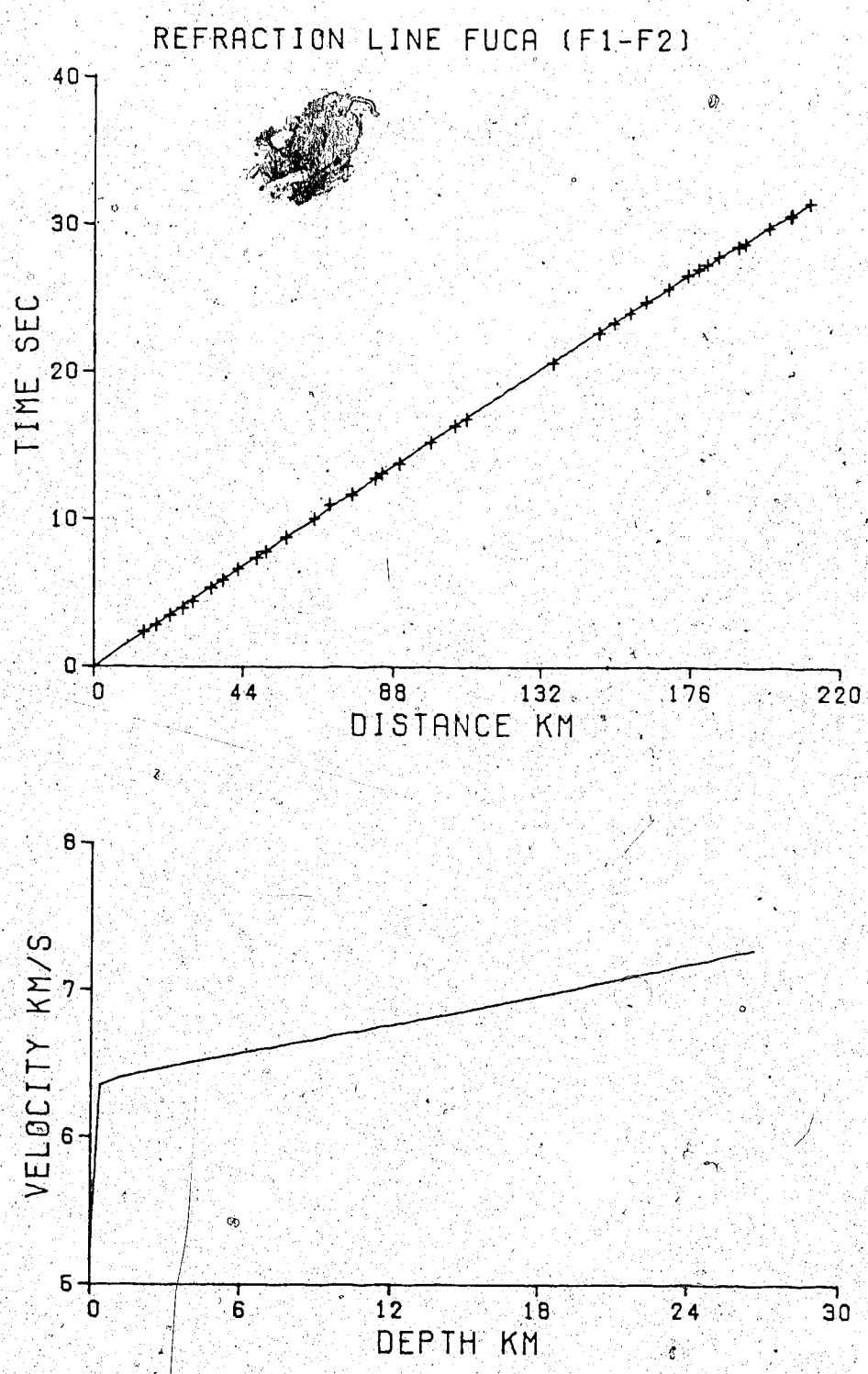

Figure 5.11 Time-distance curve: cross= raw data; solid line= data fitted by a polynomial, and the velocity-depth curve by the WHB inversion of time-distance curve beneath the surface layer.

different from the ray path that travels from A to N. One possible explanation of the discrepancy of travel times in the southerly and northerly directions is the existence of a zone of anomalous structure south of the shot point A. If this hypothesis is true, it might account for some of the discrepancies in the travel-time curves. The extent of the anomalous zone cannot be estimated precisely from the refraction data of the present study.

5.6 Synthetic Seismograms

The interpretation based on travel-time analysis alone is not always unique, and a comparison of theoretical and experimental travel-time curves can be useful to avoid mistakes in the solution of an inverse problem. The theoretical travel times can be approximated by modified asymptotic wave methods (Cervery and Zahradnik, 1972; Choi, 1978).

The method used to compute time-distance curves in the present study is based on a modified Airy function solution derived by Choi(1978). His approach was to derive a integral solution for an arbitrary ray in a layered, vertically inhomogeneous elastic medium, using a modified version of a third-order saddle point approximation. This result was then reduced to the form of a modified Airy function solution for the computation of a synthetic seismogram. For a detailed analysis the reader is referred to Choi(1978).

Since we anticipate lateral velocity variations and the existence of a low velocity zone as suggested by the first arrival data, we do not expect that all the features on the observed record section can be matched by a modelling procedure using synthetic seismograms. In general, the theoretical computations provide an approximate velocity-depth structure which is at least consistent with the observed travel-time and amplitude data.

The construction of the synthetic seismogram was initially based on the velocity-depth function of the Fuca profiles (F1-F2) which was derived from the WHB inversion of travel times. The parameters, velocity as well as depth, of the synthetic seismogram were adjusted to fit with the observed data of the Fuca profiles. The data to be fitted by the synthetic seismogram include the refractions from the crust and from the mantle, and reflections from the mantle. In order to improve the fit of the observed data, a low velocity zone was required to keep the reflected travel times correct at larger distances and to generate the large amplitudes of the possible Moho reflections described above. The Moho reflections from the synthetic seismogram fitted very well to observed data of the Fuca profile (in Fig. 5.6). The critical distance from the synthetic calculation was at 140 km. Unfortunately, the synthetic seismogram program was not designed to compute the theoretical travel times of the Pn phase branch, however, the theoretical Pn travel times may be estimated from the critical distance as

determined from the synthetic seismogram with the assumptions of a horizontal Moho discontinuity and a mantle velocity of 8.0 km/s (rounded off from the observed velocity of 7.95 km/s). The observed Pn arrival times are approximately one second earlier than those predicted by the above model. We then varied the velocity and the thickness of the low velocity zone in an attempt to improve the fit of the Pn arrivals. This attempt failed. We could fit either the reflected or refracted branch from the Moho discontinuity to the observed data, but were unsuccessful in fitting both simultaneously.

Since we anticipate lateral velocity variations beneath Vancouver Island, the assumptions of a horizontal Moho discontinuity and a constant velocity over 100 km may not be valid for the computation of the theoretical travel times of Pn arrivals. Significant lateral velocity variations may account for the early Pn arrivals of the observed data. Another plausible reason is dip on the Moho discontinuity. A few degrees of dip over 100 km is sufficiently large to produce time shifts of the magnitude required to bring reflected and refracted phases into an agreement. Since the Pn arrivals in the Nero profile (reversed profile) can not be identified, the determination of the dip angle is not possible. If the Moho discontinuity has dip, the observation of the earlier Pn arrivals requires the waves to propagate in the updip direction, i.e. the Moho interface is dipping from the northern end towards the southern end of the

island. We may estimate the magnitude of time shifts caused by the effect of dip angle by considering a dipping two-layer structure. We assume the upper layer velocity to be 6.5 km/s, and lower layer velocity to be 8.0 km/s. Only about 3.0 degrees of dip is required to produce approximately 1.0 sec to 1.5 sec time-shift difference between the two-layer horizontal and dipping model, at distances 200 km to 300 km from the shot. If the Moho beneath Vancouver Island has 3 degrees of dip, its true velocity will become approximately 7.7 km/s.

The model that produced the best fit to the observed refractions from the crust and reflections from the mantle for the Fuca profiles has following features: 1. the velocity increases continuously to a depth of 27 km; 2. below this depth the velocity gradually decreases to 6.2 km/s at the depth of 38 km; 3. the low velocity zone stays constant at 6.2 km/s for a thickness of 6 km and sharply jumps to a velocity of 8.0 km/s. Fig.5.12 shows the ray diagram and travel-time curves of this model. The travel-time curves generated by this model agree very well with the observed data. This model provides an alternative interpretation which may be compared to the plane-layered model derived earlier.

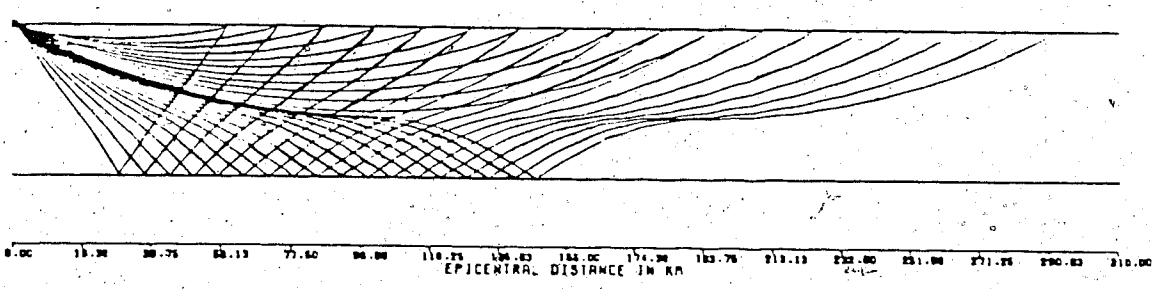

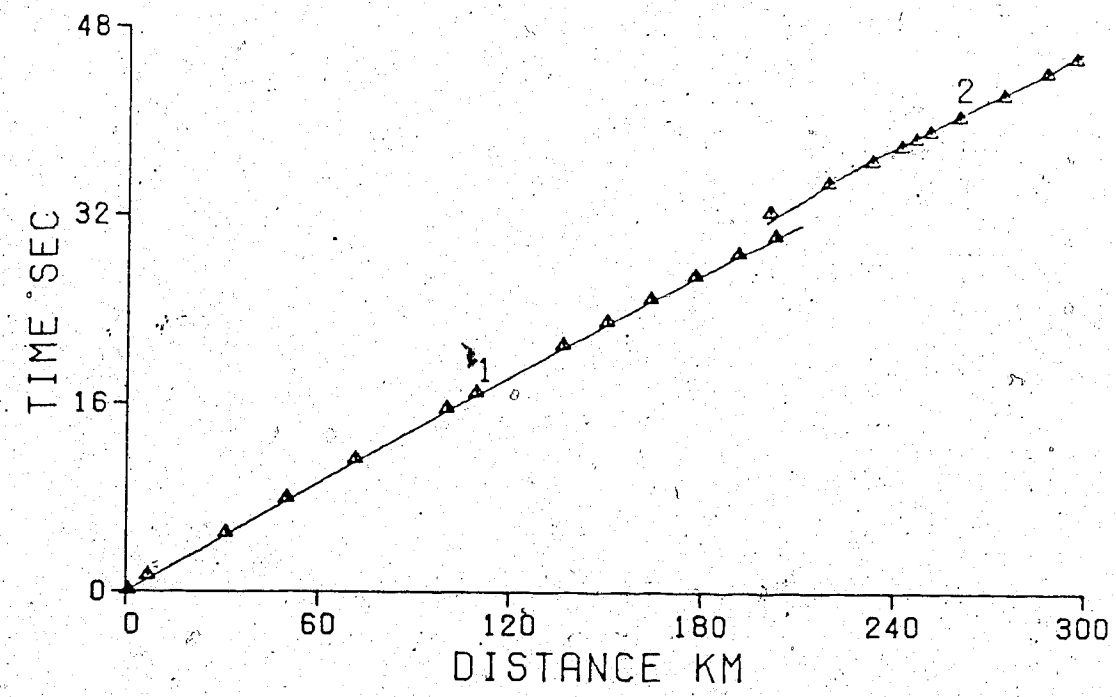

Figure 5.12 Synthetic ray diagram and corresponding travel-time curves for the Fuca profile: solid=observed, triangle=computed; branch 1= refractions from the crust, branch 2= reflections from the mantle.

5.7 Particle Motion Analysis

Particle motion diagrams may be constructed by plotting the radial and vertical seismometer signals as a function of time for the first arrival data. The orientation of the principal axis of the particle trajectory in the radial-vertical plane indicates the apparent angle of emergence of the refracted wave. Montalbetti (1969) and Kazmierczak (1980) provided good discussions of particle motion analyses of both compressional and shear type motions.

Three components of ground motion (vertical, north-south horizontal, and east-west horizontal) for all shots, were recorded at a few stations in Vancouver Island. All component data were recorded on the Sprengether and U. of A. digital array systems. Unfortunately, the information from the U. of A. digital array were not applicable for particle motion analysis either because of noisy data or dead traces. Thus, the analysis was based only on the data recorded by the Sprengether system from four different shot points.

The radial component is obtained by rotating the two horizontal components into a direction corresponding to a great circle azimuth from source to receiver. The azimuth is the angle measured clockwise from the north. Two methods were used to estimated the azimuth:

1. Theoretical calculation of azimuth from the geometry of both source and receiver coordinates.

2. Direct measurement of azimuth from the plot of the north-south and east-west horizontal components.

The maximum difference of the azimuth obtained from both methods is up to 20 degrees. We decided to use the azimuth measured from the plot of north-south and east-west components to transform to radial motion because we believed that the orientation of the detectors in the field was only approximately in the north-south direction, and that the measured azimuth was more reliable than the azimuth computed by the theoretical calculation.

Fig.5.12 to 5.16 show the first arrival events of three horizontal components and one vertical component for different shot locations. It is obvious that P-wave type motion is present in all records. The apparent angle of emergence measured from the horizontal varies from 31 to 51 degrees.

Since the tilt angle of the principal axis of the particle trajectory is equivalent to the apparent angle of emergence of the refracted wave, we could make use of amplitudes Av and Ah of the vertical and horizontal ground displacement to measure the apparent angle of emergence which is defined as

$$\alpha = \tan^{-1} (Av/Ah)$$

where: α is the apparent angle of emergence measured with horizontal boundary. Walker (1919) derived a relation between the apparent and true angle of emergence in the form

$$2\cos^2\beta = (1-\gamma)/(0.5-\gamma)(1-\mathrm{Sin}\alpha)$$

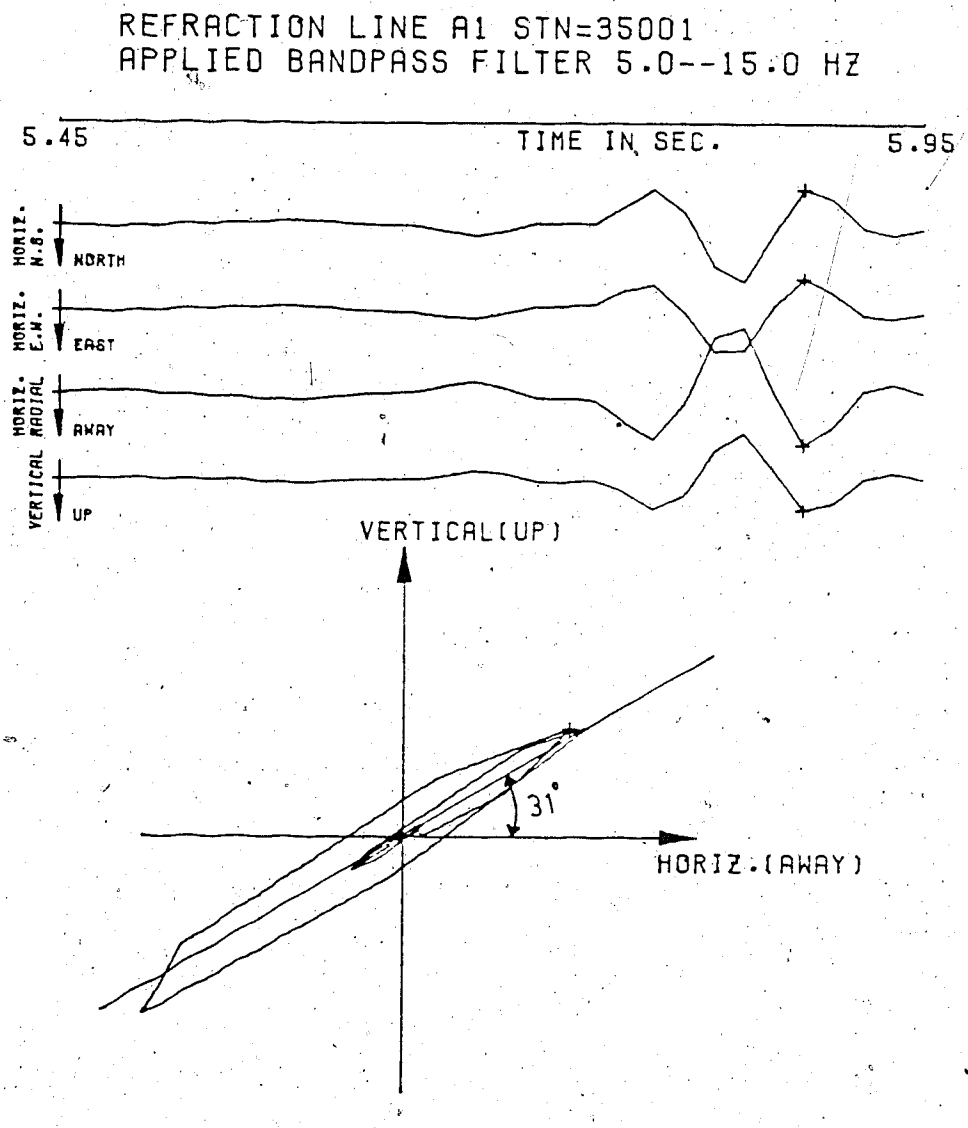

Figure 5.13 Plots of four components of ground motion and radial versus vertical ground motion. The apparent angle of emergence from horizontal boundary is 31°.

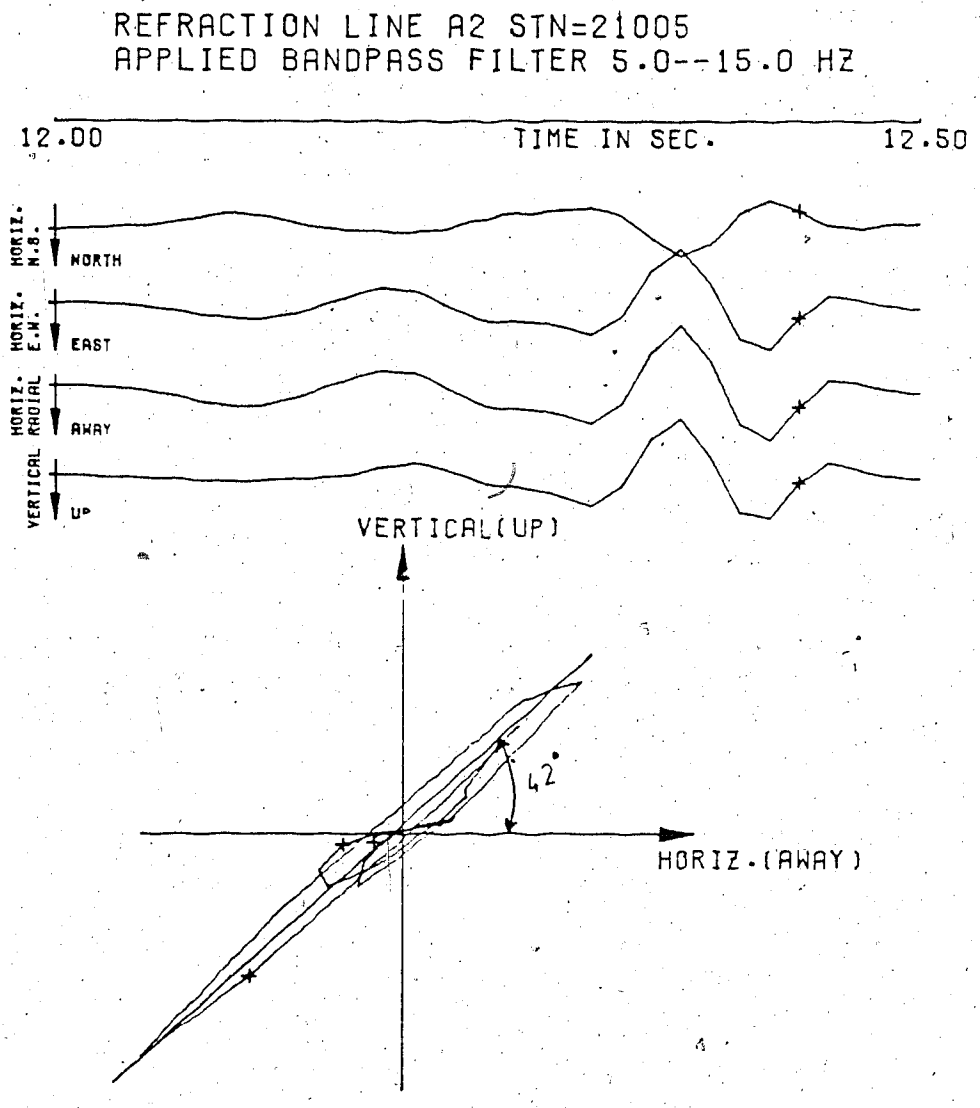

Figure 5.14 Plots of four components of ground motion and radial versus vertical ground motion. The apparent angle of emergence from horizontal boundary is 42°.

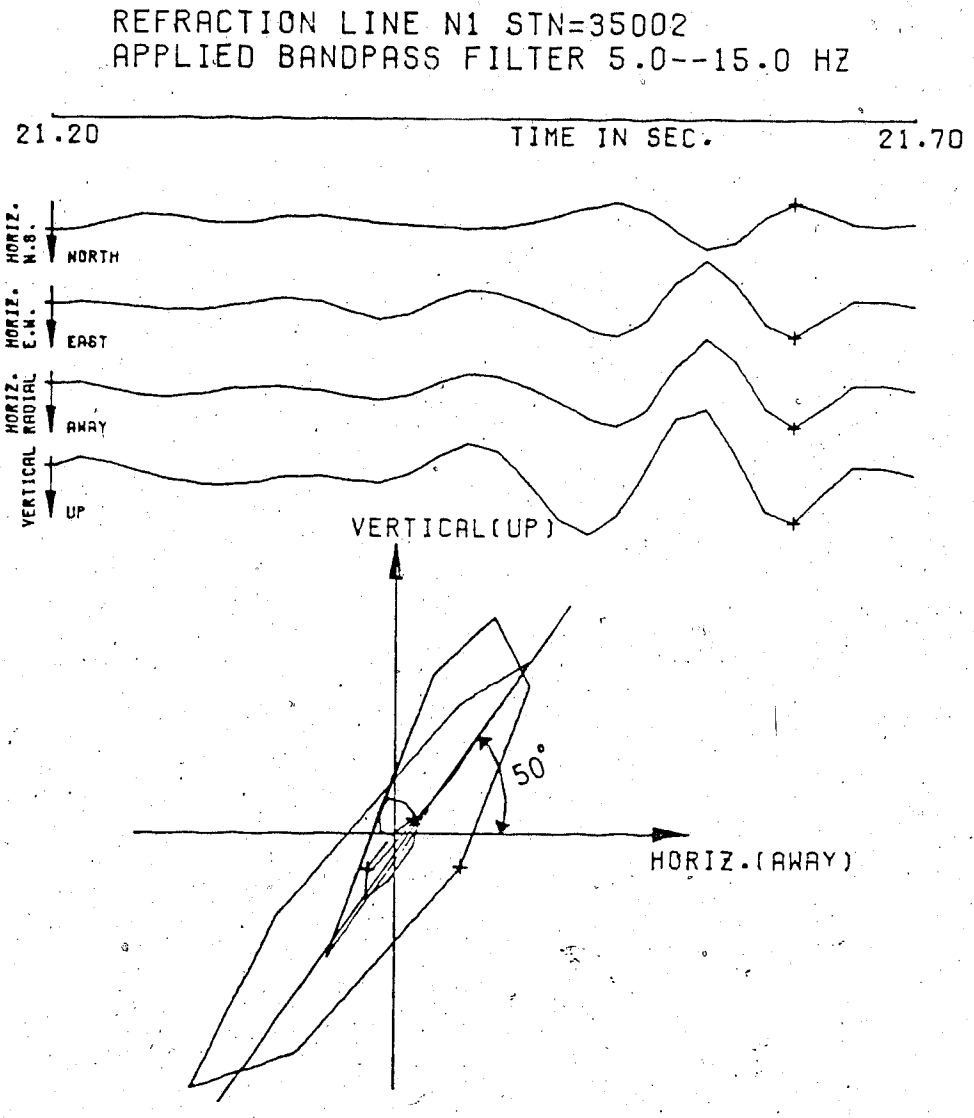

Figure 5.15 Plots of four components of ground motion and radial versus vertical ground motion. The apparent angle of emergence from horizontal boundary is 50°.

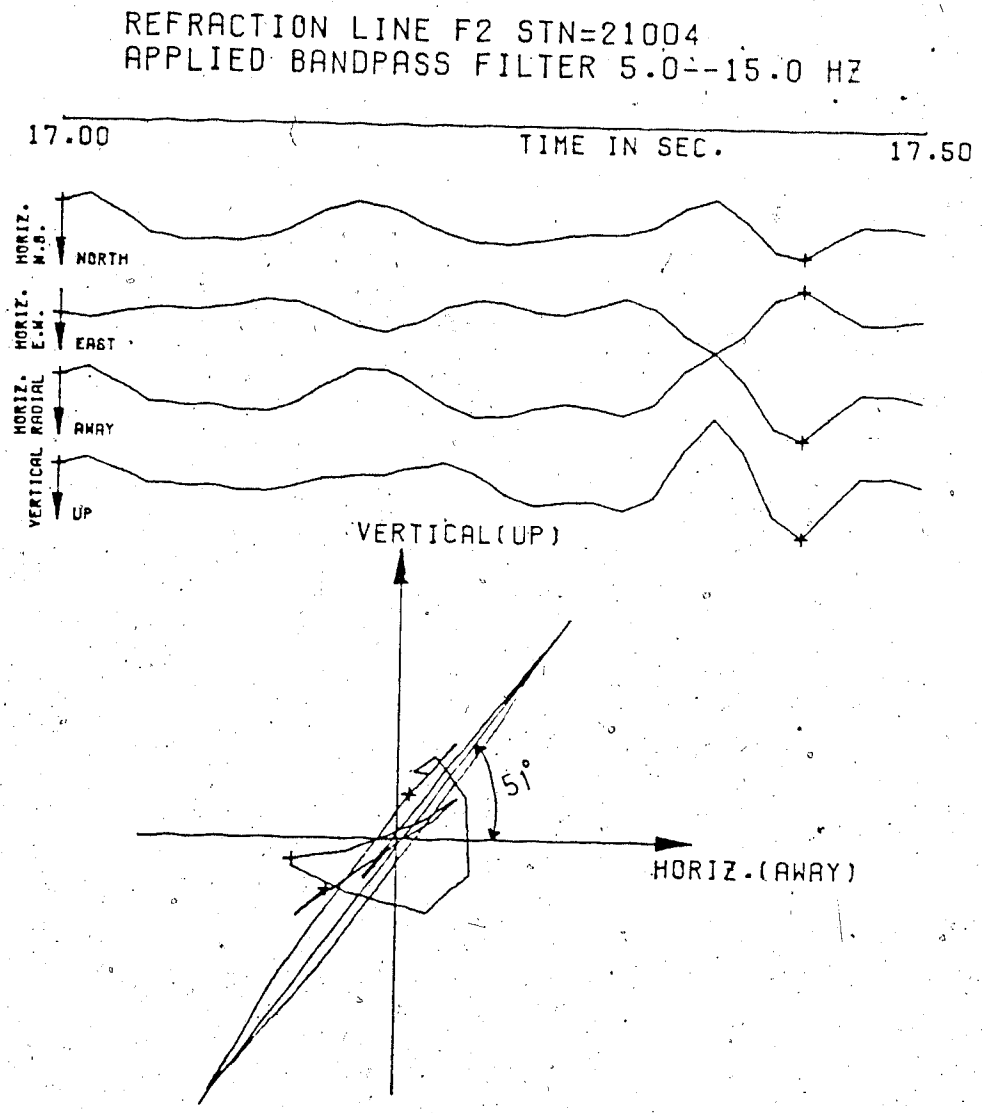

Figure 5.16 Plots of four components of ground motion and radial versus vertical ground motion. The apparent angle of emergence from horizontal boundary is 51°.

where:

γ = Poisson's ratio,

β = angle of emergence measured from the horizontal.

Cumming, Clowes and Ellis (1979) concluded that Poisson's ratio in British Columbia was 0.23. This value was adopted to compute the true angle of emergence. This Poisson's ratio may be in error when it is applied to data from Vancouver Island. Mereu (1966) showed that an increase of Poisson's ratio from 0.2 to 0.3 had the effect of increasing the apparent angle of emergence a few degrees (the maximum was about 7 degrees). Thus we conclude that Poisson's ratio is not a critical factor in the determination of angle of emergence in our case.

By knowing the velocity of the wave at the bottom of the trajectory from the travel-time analysis, we can estimate the near surface velocity by Snell's law.

$$\sin(i) = V_0/V_1$$

where:

i = the angle of emergence with respect to the normal,

V_0 = near surface velocity,

V_1 = velocity at the maximum depth of penetration.

The apparent angles of emergence from all particle motion diagrams were measured, and then converted to true angles of emergence measured from the vertical in order to compute the near surface velocities (Table 3).

From Table 3 the surface velocity fluctuates from 4.0 to 5.27 km/s in this particle motion analysis. The

line	geophone station	measured azimuth (degree)	angle of emergence (degree)	velocity particle analysis km/s	velocity plane layer km/s
A1	35001	40	56.3	5.27	5.28
A2	21005	300	43.4	4.4	4.57
N1	35002	307	35.3	4.0	---
F2	21004	132	35.0	4.0	5.33

Table 3.... Near surface velocities from the particle motion analyses compared with those from plane-layered interpretation.

uncertainty of Poisson's ratio, error of the azimuth, and the assumption of a homogeneous, isotropic, elastic medium definitely contribute certain errors in obtaining the surface velocities at various locations. When the errors and assumption are taken into consideration, the surface velocities from particle motion analysis are considered to agree with velocities from the travel-time analysis based on the travel time to the first detector. Since the available data are limited and the surface velocities from the travel-time analysis are not well defined, it may be justified to use the velocity of 4.0 km/s from particle motion analysis as a lower bound for the surface velocity and 5.33 km/s from travel-time data as a upper bound.

6. INTERPRETATION

6.1 Introduction

The prime objective of this study is to obtain crustal structural information under Vancouver Island. Interpretations of crustal structure in this thesis are based on the analysis of refraction data through the application of horizontal, plane-layered models, and through the inversion of travel-time curves by the WHB integral and includes synthetic modelling of travel-time branches. The interpreted results of four crustal seismic sections evaluated by each technique are combined to provide two preliminary models in the study area. Comparison of the two methods indicates that the model obtained by the WHB integral technique seems to represent a more realistic model than the horizontal-layered interpretation.

6.2 A Preliminary Model from Plane-layered Intrepretation

By combining the results of the individual seismic sections from the plane-layered interpretation, a tentative regional crustal model may be constructed for the study area. Because of limitations of the data and the large separation distances between recording sites, this model should be regarded as speculative at this time.

Fig.6.1 shows the inferred crustal model. This consists of 4 horizontal layers. The low velocity surface layer is

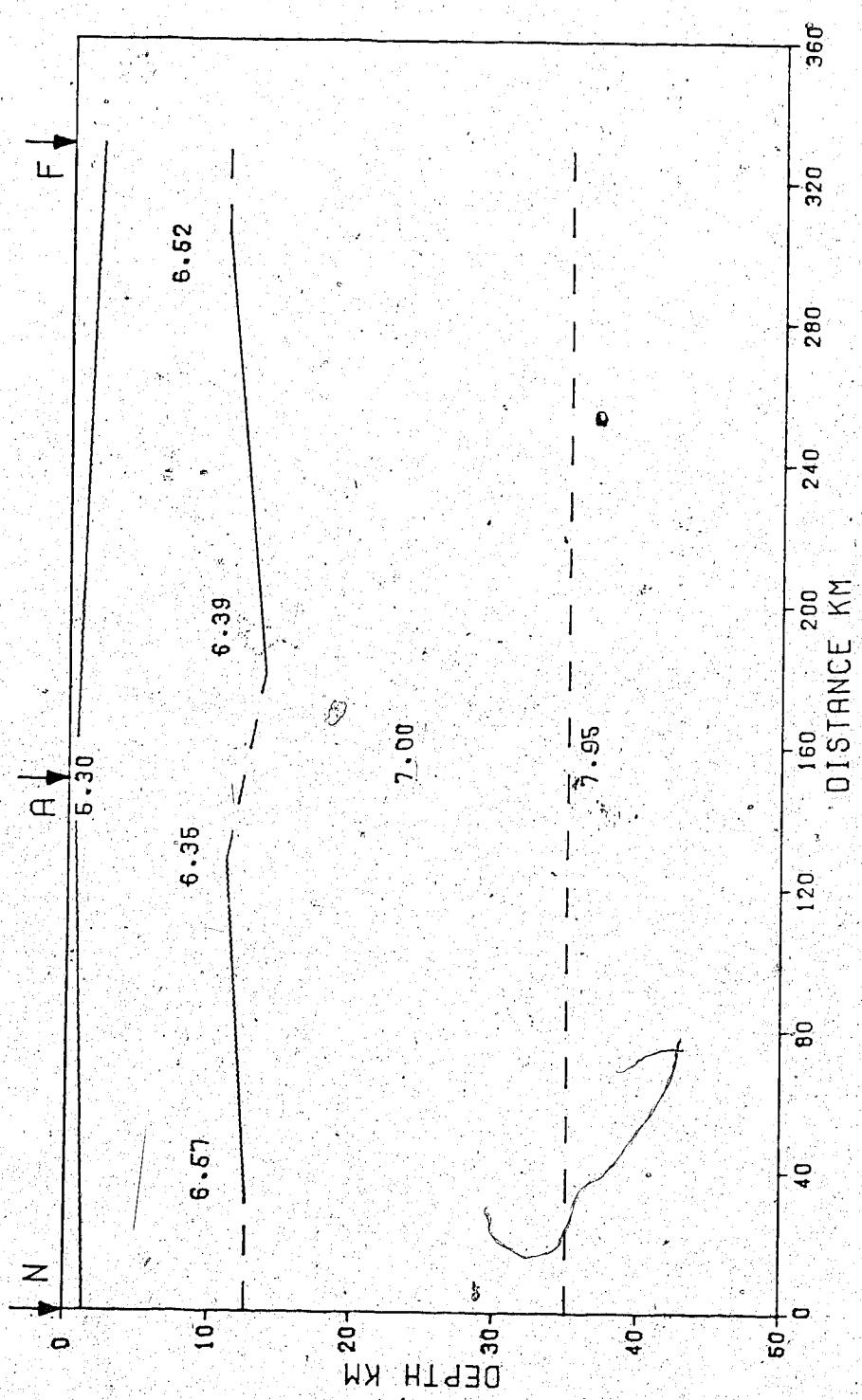

Figure 6.1 A velocity model from plane-layered interpretation along the profile lines in Fig.3.1. Contours are velocity in km/s. Shot points are marked with arrow. Reliability of the contours is: solid line=good, dashed lines=poor.

thin towards the centre of the profile, and become thicker at both ends. The maximum thickness of "sediments" is about 2.1 km at the south end and the minimum is 0.51 km at the centre.

The depth as well as velocity above the 7.0 km/s refractor shows quite substantial changes across the profile. The velocity, proceeding from both ends of the profile towards the centre, decreases from approximately 6.5 km/s to 6.35 km/s, and there is a significant increase of thickness towards the centre. These lateral variations of velocities and thicknesses may suggest a disturbed zone or a zone of major changes in rock compositions across the central profile. On the whole, the upper crust is relatively homogeneous except at the centre of the profile.

The observed discontinuity of Pn arrivals certainly obscures the interpretation of the Moho arrivals. This discontinuity can be interpreted as indicating the existence of a low velocity zone beneath the 7.0 km/s refractor. If such a low velocity zone is present, the interpretation based on plane-layered models may produce serious error in estimating the Moho depth, because it violates the basic principle of plane-layered modelling in which velocity should increase with depth. However, the observations of Pn arrivals on profile F1 provide an indirect way to estimate the depth of the Moho. Unfortunately, the high noise levels on the reversed profile make the picks of the first arrivals very difficult, thus the velocity and depth of the Moho are

not well constrained by the refraction data. Since we speculate the existence of the low velocity zone, the Moho depth (35 km) by plane-layered interpretation should be regarded as tentative at this time, and probably represents a minimum crustal thickness.

6.3 A Preliminary Model From the Synthetic Seismogram and WHB Inversion of Travel Times

The interpreted results from the WHB inversion of travel times and synthetic seismogram modelling were also combined to form a tentative interpretation in Fig.6.2. The construction of this model was based on the following assumptions:

1. The thicknesses of surface "sediments" were taken from the plane-layered interpretation.
2. The velocity increases continuously with depth to about 7.0 km/s at a depth of approximately 17 km. The depth to this refractor was derived by combining the velocity-depth functions of four seismic sections.
3. The WHB inversion of travel-time data up to a distance of about 210 km from the Fuca profiles yielded a maximum velocity of 7.30 km/s at a depth of 27 km.
4. A transition zone was introduced beneath the 7.3 km/s refractor by synthetic modelling. The velocity in the transition zone decreases gradually from 7.3 km/s to 6.2 km/s at the depth of 38 km.

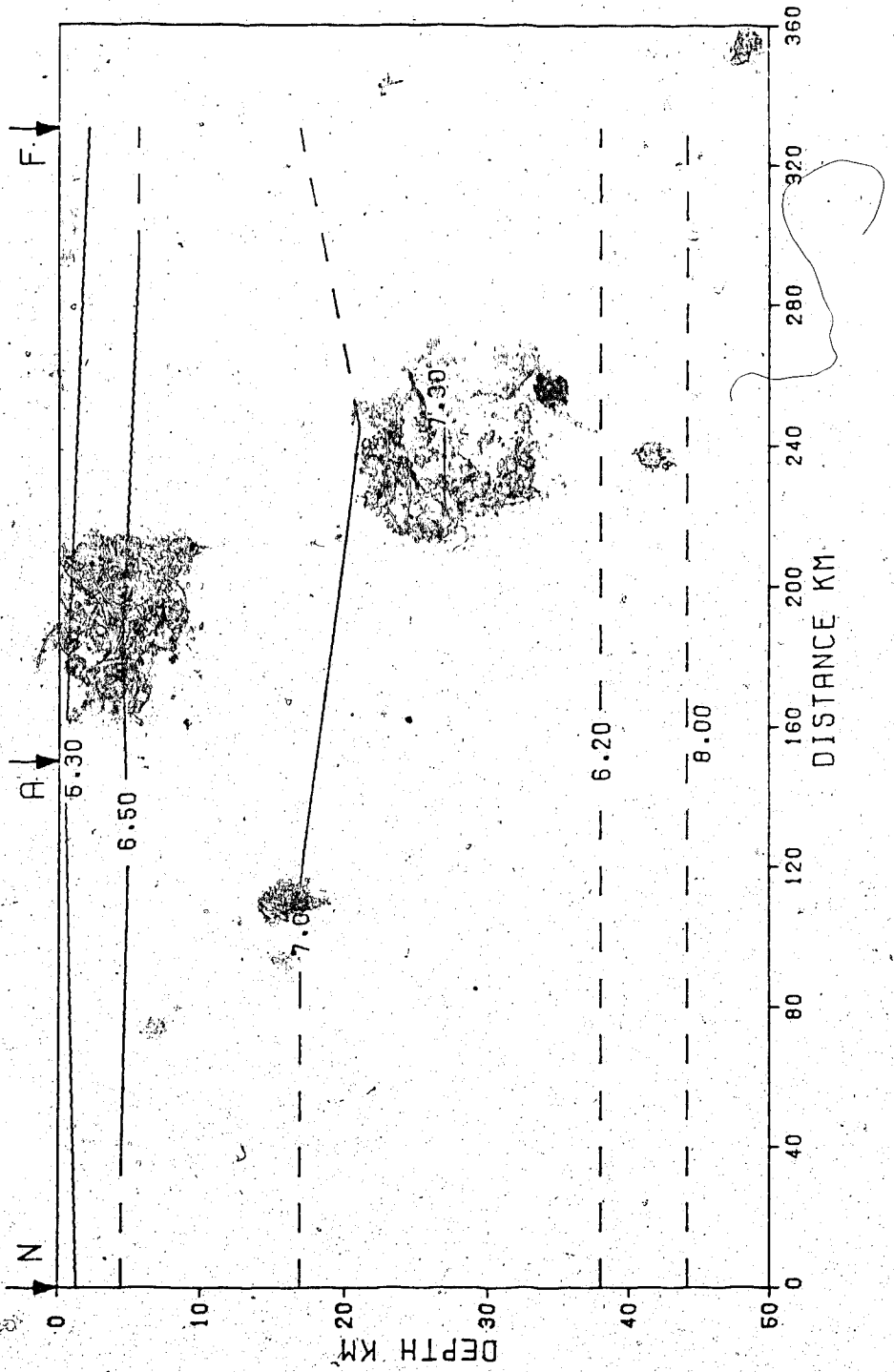

Figure 6.2 A velocity model from synthetic seismogram and WHB inversion of travel times along the profile lines in Fig.3.1. Contours are velocity in km/s. Shot points are marked with arrow. Reliability of the contours is: solid line=good, dashed lines=poor.

5. The low velocity of 6.2 km/s stays constant for a thickness of 6 km and sharply jumps to a velocity of 8.0 km. This low velocity channel was introduced in order to account for the large amplitude events which may be Moho reflections.

This model in Fig. 6.2 exhibits a different crustal structure compared to Fig. 6.1. The thickness of the 6.5 km/s refractor is fairly constant along the whole profile in Fig. 6.2. There are slight variations of thicknesses south of the shot point A. The lack of structural variation may suggest that the structure down to the 6.5 km/s refractor is fairly homogeneous.

At the depth about 17 km the 7.0 km/s refractor is fairly horizontal at both ends of the profile, but the depth varies substantially near the south of location A, in which the variation of depths is well represented by an apparent syncline. The difference in depth determined from southern profile to the northern profile is up to 4 km. This indicates that the ray path that travels from A to F is considerably different from the ray path that travels from A to N. One possible explanation to this large discrepancy in depth is due to a local, anomalous structure south of shot point A. However, if this anomalous structure exists, the refaction data in this study do not provide enough information to determine the extent of this zone, therefore this interpretation is to some extent arbitrary because of significant lateral inhomogeniety.

Besides the uncertainty in the depth to the 7.0 km/s refractor, the observation of a discontinuity in travel times contributes another uncertainty to estimate the depth of the Moho. Langston (1981) concluded the existence of a low velocity zone beneath Vancourer Island. This evidence provides further support to our present model. Although the thickness of the low velocity zone and the depth to the Moho (44 km) were found by synthetic modelling, both should be considered to be speculative at the present time. Further seismic surveys are required to establish a well-defined depth of the Moho.

6.4 Comparison of Two Models

Comparsion of the models in Fig. 6.1 and Fig. 6.2 shows that the depth to each refracting layer from the plane-layered model is less than the depth from the WHB inversion of travel times. For example, the maximum difference in depth to the 7.0 km/s refractor is up to about 7.3 km. This result seems to be quite reasonable, for the WHB integral takes into consideration velocity increases with depth and this should give a thicker section than that obtained by assuming a constant velocity. In the real geological situation, the assumption of velocity increasing with depth is presumably more realistic than the assumption of constant velocities in a small number of layers. The observed discontinuity of travel times on the Fuca profiles

certainly favors the model in Fig. 6.2 which accounts for the low velocity zone indicated by the travel-time discontinuity. In addition, a structural interpretation based on an iterative modelling of the reflected and refracted P-wave travel times and amplitudes (McMechan and Spence, 1982) indicates a crustal model similar to that in Fig. 6.2. The depths to both 6.5 km/s and 7.0 km/s refractors are consistent for both models, but the model from McMechan and Spence has a very complex structure near the centre of the profile. Based on this evidence, the model obtained by combining the synthetic seismogram and the WHB inversion of travel times is preferred as the final model in this study.

7. CONCLUSIONS

The limited extent and the nature of the data in the present investigation restrict any conclusions to only provisional comments. The overall paucity of observations of Pn arrivals for Vancouver Island also limits any possible conclusions about the regional crustal structure. However, if the features of Fig. 6.2 represent the general structure for the region, several conclusions can be made:

1. The surface "sediments" (low velocity materials) are thinner towards the centre of the profile.
2. The upper crust to a depth of about 5 km is well constrained by the reversed refraction data and has a homogeneous velocity.
3. The depth to the 7.0 km/s refractor shows substantial change of crustal thicknesses to the south of location A. This suggests the existence of a locally anomalous structure in that region.
4. Although refracted arrivals from the Moho have been identified, its depth and shape remain uncertain, however, a depth of 44 km with a mantle velocity near 8.0 km/s is reasonably consistent with the data.

The refraction data in the present study provide indirect information as to the crustal thickness beneath Vancouver Island. In attempting to interpret the refraction data to obtain the lower crustal and upper mantle structures under Vancouver Island, we feel that the interpretation of the present data is somewhat

arbitrary and less reliable than would be desirable. The limitations in this case are mainly due to a lack of seismic control along the refraction profiles particularly at large distances, and the complex structure beneath Vancouver Island. Larger shots and closer spacing of recording sites are suggested to obtain reliable Moho arrivals for further studies. If a low velocity zone exists at depth, even a more detailed refraction interpretation may be ambiguous. An indication of complex structure particularly in the centre of the Island and the possibility of a low velocity zone at [redacted]pth might be resolved by a near-vertical reflec[redacted]study.

BIBLIOGRAPHY

Alsopp,D.F.,Burke,M.D.,and Cumming,G.L.,1972, A digital seismic recording system, Bulletin of the Seismological Society of America, 62, no.6, p.1641-1647.

Barr,K,G.,1971. Crustal refraction experiment: Yellowknife 1966., J.Geophys. Res.,76, p.1929-1947.

Båth,M.,1974. Spectral analysis in geophysics, Elsevier Scientific Company,new york,chap 3-6.

----- 1979. Introduction to seismology, Birkhauser Verlag Basel, Boston, Stuttgart, p. 254-256.

Berry,M.J.and Forsyth,D.A., 1975. Structure of the Canadian Cordillera from seismic refraction and other data, Can. J. Earth Sci., p.182-208.

Cervery,V. and Zahradnik,J.,1972. Amplitude-distance curves of seismic body waves in the neighborhood of critical points and caustics-- A comparison, Z.Geophys, 38, p. 499-516.

Choi,A.P.,1978., Rays and Caustics in vertically inhomogeneous elastic media, Unpubl. M.Sc. thesis,

University of Alberta, Edmonton, Alberta.

Crosson,R.S.,1972. Small earthquakes,structure and tectonics of the Puget Sound region, Seismological Society of America Bulletin,62,p.1133-1171.

Cumming,G.L. and Kanasewich,E.R., 1966. Crustal structure in Western Canada, Final Report,May 1, 1963- April 30, 1966. Advanced Research Projects Agency, Contact AF19(628)-2835, Task no. 865202, Document no. AFCRL-66-519, p.1-126.

Cumming,W.B., Clowes,R.M., and Ellis,R.M., 1979. Crustal structure from a seismic refraction profile across southern British Columbia, Can. J. Earth Sci.,16, p.1024-1031.

Dickins,D.G.,1973. Least squares inverse filtering of seimic reflection data, Unpubl. M.Sc. thesis, University of Alberta, Edmonton, Alberta, p.70-76.

Dobrin,M.B., 1976. Introduction to geophysical prospecting, Third edition, McGraw Hill, Toronto, Ont. p. 137.

Ellis,R.M. and Clowes,R.M., 1981. Acquisition and interpretation of crustal reflection/refraction data across Vancouver Island, Earth Physics Branch Open File

Report 8-11, p. 72.

Grant,F.S. and West,G.F., 1965. Interpretation theory in applied geophysics, McGraw Hill Company,New York.

Hales,A.L. and Nation,J.B., 1973. A seismic refraction survey in the northern Rocky Mountains: more evidence for an intermediate crustal layer, Geophys. J. Roy. Astro. Society, 35, p.381-399.

Hyndman,R.D., 1976. Heat flow measurements in the inlets of southwestern British Columbia, J. Geophys. Res.,81, p.337-349.

Hyndman,R.D., Riddihough,R.P., and Herzer,R., 1979. The Nootka fault zone --new plate boundary off Western Canada, Geophys. J. Roy. Astro. Soc. 58, p.667-683.

Jakosky,J.J., 1950. Exporation geophysics, Trija publishing company, Calif., p.750-755.

Kanasewich,E.R., 1975. Time sequence analysis in geophysics, Second edition, University of Alberta Press, Edmonton, Alberta.

Kazmierczak,Z., 1980. Seismic crustal studies in Saskatchewan, Unpubl. M.Sc. thesis, University of

Alberta, Edmonton, Alberta, p.64-72.

Keen,C.E. and Hyndman,R.D., 1979. Geophysical review of the continental margins of eastern and western Canada, Can. J. Earth Sci.,16, p.712-747.

Langston,C.A., 1981. Evidence for the subducting lithosphere under southern Vancouver Island and Western Oregon from teleseismic P wave conversions, J. Geophys. Res., 86, p.3857-3866.

Lubkin,Y.J., 1970. Filter systems and design: electrical, microwave, and digital. Addison-Wesley publ. company, Ontario, p.76-84.

McKenzie,D.P. and Sclater,J.G., 1968. Heat flow inside the island arcs of the northwestern Pacific, J. Geophys. Res.,73, p.3137-3170.

McMechan,G.A. and Spence,G.D., 1982. P-wave velocity structure of the earth's crust beneath Vancouver Island (Manuscript to be subsmitted for publication).

Mereu,R.F. and Hunter,J.A., 1969. Crustal and upper-mantle structure under the Canadian shield from Project Early Rise data, Bull. Seismol. Soc. Am.,59, p.147-155.

Monger,J.W. and Price,R.A., 1979. Geodynamic evolution of the Canadian Cordillera- progress and problems, Can. J. Earth Sci., 16, no.3 p.770-791.

Montalbetti,J.F., 1969. Broad-band digital seismic data analysis, Unpubl. M.Sc. thesis, University of Alberta, Edmonton, Alberta, p.50-59.

Muller,J.E., 1974. Victoria map-area, Pacific Rim National park, Vancouver Island, B.C., Geol. Surv. Can., paper 74-1A, p. 21-23.

----- 1977. Evolution of the Pacific margin, Vancouver Island, and adjacent regions, Can. J. Earth Sci.,14, p.2062-2085.

Overton,A., 1970. Seismic refraction measurement surveys; western Queen Elizabeth Islands and polar continental margin, Can. J. Earth Sci.,7, p.346-365.

Rankin,D.S., Ravindra,R., and Zwicker,D., 1969. Preliminary interpretation of the first refraction arrivals in Gaspe from shots in Labrador and Quebec, Can. J. Earth Sci.,6, p.771-774.

Riddihough,R.P., 1978. The Juan De Fuca plate, Transactions, Amer. Geophys. Union, 59, p. 836-842.

----- 1979. Gravity and structure of an active

margin-British Columbia and Washington, Can. J. Earth Sci., 16, p.350-363.

Robinson,E.A. and Silvia,M.T., 1979. Deconvolution of geophysical time series in the exploration for oil and natural gas, Elsevier Scientific publ. company, New York, p.215-218.

Rogers,G.C., 1979. Earthquake fault plane solutions near Vancouver Island, Can. J. Earth Sci., 16, p.523-531.

Tseng,K., 1968. A new model for the crust in the vicinity of Vancouver Island. Unpubl. M.Sc. thesis, University of British Columbia, Vancouver, British Columbia.

Walker,G.W., 1919. Surface reflection of earthquake waves, Phil. Trans. Roy. Soc. (London) A,218, p.373-393.

White, W.R. and Savage,J.C., 1965. A seismic refraction and gravity study of the earth's crust in British Columbia, Bull. Seismol. Soc. Am., 55, p.463-486.

Wicken,A.J., 1977. The upper mantle of southern British Columbia, Can. J. Earth Sci., 14, p.1100-1115.

APPENDIX ---COMPUTER PROGRAMS

```
C
C
C     THIS PROGRAM COMPUTES THE AMPLITUDE AND PHASE SPECTRA
C     OF UNIVERSITY OF ALBERTA RECORDING SYSTEM AND
C     SEISMOMETER IN 1980 SEISMIC PROJECT IN VANCOUVER
C     ISLAND.
C
C     FQ    = FREQUENCY VECTOR OF THE SPECTRUM
C     AMP   = AMPLITUDE VECTOR OF THE SPECTRUM
C     PHASE = PHASE ANGLE VECTOR OF THE SPECTRUM
C     TRANS = TRANSFER FUNCTION OF AMPLIFIER AND
C             SEISMOMETER IN S-PLANE REPRESENTATION
C
C
      DIMENSION FQ(81),BLOGF(100),AMP(100),BLOGA(100)
      DIMENSION TITLEX(60),TITLEY(60)
      DIMENSION BLOGAM(100),PHASE(100)
      COMPLEX A,I,S,TRANS
      COMMON TITLEX,TITLEY,NTITLX,NTITLY,AXLEN,AYLEN
C
C  SEE THE EXPLANATION OF VARIABLES IN SUBROUTINE PLOTA.
C
      READ(5,111) TITLEX
      READ(5,111) TITLEY
  111 FORMAT(60A4)
      WRITE(6,111)TITLEY
      READ(5,112)AXLEN,AYLEN
  112 FORMAT(2F6.0)

      READ(5,113)NTITLX,NTITLY
  113 FORMAT(2I6)
C  ***********************************************
      I=(0.0,1.0)
      ARC=6.283185
C
C  FMIN=THE MINIMUM FREQUENCY
C  FMAX=THE MAXIMUM FREQUENCY
C  FACTOR=THE GAIN OF THE AMPLIFIER (58DB)
C
      READ(5,4)FMIN,FMAX,FACTOR
    4 FORMAT(3F9.4)
      NN=1
      FREQ=FMIN
  100 S=I*FREQ
      FQ(NN)=FREQ
C
C  TRANS= THE TRANSFER FUNCTION OF AMPLIFIER +SEISMOMETER
C
      A=TRANS(S)
      AMP(NN)=CABS(A)
      PHASE(NN)=ATAN2(AIMAG(A),REAL(A))*360./ARC
```

```
      BLOGF(NN)=ALOG10(FREQ)
C
C  CONVERT AMPLITUDE INTO DECIBEL
C
      BLOGA(NN)=ALOG10(AMP(NN))*20.0+FACTOR
      BLOGAM(NN)=ALOG10(AMP(NN))
      WRITE(6,18)FREQ,AMP(NN),BLOGAM(NN),PHASE(NN)
   18 FORMAT(4(1X,F11.4))
      FREQ=FREQ*1.1547820
      NN=NN+1
      IF (FREQ.LE.FMAX)GO TO 100
      N1=NN-1
      CALL PLOTA(BLOGF,BLOGAM,N1)
      STOP
      END
C
      COMPLEX FUNCTION TRANS(S)
      COMPLEX S
      TRANS=(1)
     1 ((S/.10)/(1.0+S/.10))*1.0/(1.0+1.2*S/4700.
C     THE TRANSFORMER
     1 +(S/4700.)**2)*1.0/(1.0+S/53.1)
C     THE PREAMPLIFIER
     1 *(S/.100)/(1.0+S/.100)
C     THE D.C.OFFSET FILTER
     1 *1.0/(1.0+S/53.1)
C     THE GAIN CONTROL
     1 *105./(105.+105.*2.1105*S/50.+45.*(2.1105*S/50.)**2
     1 +10.*(2.1105*S/50.)**3+(2.1105*S/50.)**4)
C     THE FOUR POLE BESSEL FILTER WITH A FUDGE FACTOR
     FOR FREQUENCY
     1 *(S/2.0)**3/(1.0+.76*S/2.0+(S/2.0)**2)*8.33*10.0/
     1 (10.0+4)*2*3.1416*2
C     THE SEISMOMETER
      RETURN
      END
C
C
      SUBROUTINE PLOTA(X,Y,N)
C  REQUIRED INPUTS
C  THE TITLES OF X- AND Y- AXIS
C  AXLEN-AYLEN: DESIRED LENGTH OF X AND Y AXIS IN INCHES
C  NTITLX-NTITLY: NUMBER OF CHARS IN X-AND Y-TITLES
C  X-Y: THE VECTORS TO BE PLOTTED
C  NDATA: NUMBER OF ELEMENTS IN VECTOR X OR Y
C
      DIMENSION X(N),Y(N)
      DIMENSION TITLEX(60),TITLEY(60)
      COMMON TITLEX,TITLEY,NTITLX,NTITLY,AXLEN,AYLEN
C
C  PLOT EVERY DATA POINT
      IREP=1

      CALL PLOTS
```

```
C
C  ENLARGE OR REDUCE THE SIZE OF THE ENTIRE PLOT
      CALL FACTOR(0.8)
C
C  MOVE ORIGIN IN A BIT TO ALLOW FOR LABELS
      CALL PLOT(1.0,3.0,-3)
C
C  ENLARGE OR REDUCE THE SIZE OF THE ENTIRE PLOT
C
C  SCALE THE INPUT VECTORS
C       CALL SCALE(X,AXLEN,N,IREP)
C       CALL SCALE(Y,AYLEN,N,IREP)
C
      X(N+1)=-1.0
      X(N+2)=0.5
      Y(N+1)=0.0
      Y(N+2)=1.3333
C
C  PLOT X-AND Y- AXIS
      CALL LOGAX(0.0,0.0,TITLEX,-NTITLX,AXLEN,0.0,-1.0,
     & -3.0,3.0)
      CALL LOGAX(0.0,0.0,TITLEY,NTITLY,AYLEN,90.,-0.0,
     & -4.0,3.0)
      CALL LINE(X,Y,N,1,0,3)
C
C  TERMINATE THE PLOT
      CALL PLOT(0.0,0.0,999)
      RETURN
      END
```

```
C
C
C     THIS PROGRAM COMPUTES THE DEPTHS OF N LAYERS WITH
C     GIVEN INPUTS :
C     VELOCITIES AND INTERCEPT TIMES OF GIVEN LAYERS.
C
C     N  = NUMBER OF LAYERS TO BE COMPUTED NOT INCLUDE
C          HALF SPACE
C     NV = NUMBER OF VELOCITIES
C     TAU = THE INTERCEPT TIMES
C     AW  = VECTOR TO STORE THE TITLE OF THE LINE
C     V   = VELOCITIES OF N LAYERS
C     H   = THICKNESS OF INDIVIDUAL LAYER
C
C
      REAL TAU(10),V(10),H(10),AW(30)
      DATA TAU/10*0.0/,V/10*0.0/,H/10*0.0/
      READ(5,4)(AW(I),I=1,30)
      WRITE(6,4)(AW(I),I=1,30)
    4 FORMAT(30A4)
      READ (5,2) NV
    2 FORMAT(I1)
C
C     NOTE TAU(1) MUST BE 0.0
C
      READ(5,10)(TAU(I),I=1,NV)
   10 FORMAT(7F10.3)
      READ(5,20)(V(I),I=1,NV)
   20 FORMAT(8F9.3)
C
      DO 90 N=2,NV
      HSUM=0.0
      NLAYER=N-2
      IF(NLAYER.LE.0) GO TO 110
      DO 100 K=1,NLAYER
      V1=SQRT(V(N)**2-V(K)**2)
      V2=SQRT(V(N)**2-V(N-1)**2)
      HSUM=HSUM+H(K)*(V(N-1)*V1)/(V(K)*V2)
C     WRITE(6,101)N,K,V1,V2,HSUM
C  101 FORMAT(2I5,4F10.3)
  100 CONTINUE
C
  110 V3=SQRT(V(N)**2-V(N-1)**2)
C
      H(N-1)=TAU(N)*V(N-1)*V(N)/(2.0*V3)-HSUM
   90 CONTINUE
C
      WRITE(6,30)
   30 FORMAT('0',4X,'INTERPT TIME',5X,'VELOCITY',5X,
     & 'THICKNESS',7X,'DEPTH')
      DEPTH=0.0
      DO 40 L=1,NV
      DEPTH=DEPTH+H(L)
      IF(L.EQ.NV) DEPTH=0.0
```

```
      WRITE(6,45) TAU(L),V(L),H(L),DEPTH
45    FORMAT('0',5X,F10.3,5X,F8.3,5X,F9.3,5X,F9.3)
40    CONTINUE
      STOP
      END
```

```
C
C
C     THIS PROGRAM COMPUTES THE VELOCITY-DEPTH
C     FUNCTION FROM THE INVERSION OF TRAVEL TIMES
C     BY WHB INTEGRAL, USING A LOW ORDER POLYNOMIAL
C     TO FIT WITH THE OBSERVED TRAVEL-TIME DATA
C
C
      DIMENSION A(20),B(20),DIST(100),TIME(100),X(100)
      DIMENSION C(10),S(20),TY(100),AW(30),VEL(100)
      DIMENSION Z(500),VMAX(500),Z1(500),Y(100)
      DIMENSION RX(3),RT(3)
      COMMON AW
      REAL*8 P(200),T(200)
      DATA C/10*0.0/
C
C
C     AW   = VECTOR TO STORE THE TITLE OF REFRACTION LINE
C     RX   = DISTANCES USED TO REDUCE DATA TO THE BASE
C            OF THE SURFACE LAYER
C     RT   = TIMES USED TO REDUCE DATA TO THE BASE OF THE
C            SURFACE LAYER
C     DIST = DISTANCES OF TRAVEL-TIME DATA
C     TIME = TIMES OF TRAVEL-TIME DATA
C     TY   = TIMES COMPUTED FROM POLYNOMIAL COEFFICIENTS
C     Z    = DEPTHS CALCULATED FROM WHB INTEGRAL
C     VEL  = VELOCITIES CALCULATED FROM WHB INTEGRAL
C     N    = INPUT NUMBER OF OBSERVATIONS OF X AND Y
C     MD   = MAX DESIRED DEGREE OF THE POLYNOMIAL FIT
C     ID   = OUTPUT DEGREE OF THE FITTED MODEL
C     C    = OUTPUT COEFFICIENTS OF POLYNONIMAL FIT IN
C            ASCENDING ORDER
C     P AND T = WORKING SPACE  MUST BE DOUBLE PRECISION
C
C
      RSQ=100.
      READ(5,8)(AW(I),I=1,30)
      WRITE(6,8)(AW(I),I=1,30)
    8 FORMAT(30A4)
      READ (5,11)(RX(K),K=1,3)
      READ (5,11)(RT(K),K=1,3)
   11 FORMAT(3F10.3)
      WRITE(6,13)(RX(K),K=1,3)
   13 FORMAT('0',' RX',3F10.3)
      WRITE(6,14)(RT(K),K=1,3)
   14 FORMAT('0',' RT',3F10.3)
      READ(5,10) MD,N
   10 FORMAT(2I6)
      DO 20 I=1,N
      READ(5,25) DIST(I),TIME(I)
   25 FORMAT(2F12.4)
   20 CONTINUE
C
      CALL REDUTI(N,DIST,TIME,RT,RX)
```

```
      DO 30 I=1,N
      X(I)=DIST(I)
   30 Y(I)=TIME(I)
      TIME(1)=0.0
C
C
C     RLFOTH FROM IMSLLIB -- FIT A UNIVARIATE CURVILINEAR
C     REGRESSION MODEL USING ORTHOGONAL POLYNOMIALS
C
      CALL RLFOTH(DIST,Y,N,RSQ,MD,ID,P,C,S,A,B,IER)
C
C     RLDOPM FROM IMSLLIB -- TRANSFORMS A FITTED ORTHOGONAL
C      POLYNOMIAL MODEL INTO A POLYNOMIAL FUNCTION OF THE
C      ORIGINAL INDEPENDENT VARIABLE
C
      CALL RLDOPM(C,ID,A,B,T)
C
C     THE OUTPUT OF C CONTAINS THE CONSTANT TERM
C      AND COEFFICIENTS
C
      LD=ID+1
      DO 40 K=1,N
      CONST=C(1)
      YY=CONST
      DO 50 KK=2,LD
   50 YY=YY+C(KK)*X(K)**(KK-1)
      TY(K)=YY
   40 CONTINUE
C
      WRITE(6,60) ID
   60 FORMAT('0',5X,'DEGREE OF POLYNOMIAL FIT IS',I3)
      WRITE(6,65)
   65 FORMAT('0',15X,'THE COEFFS OF POLY. FITTED MODELS')
      WRITE(6,70)(C(K),K=1,LD)
   70 FORMAT('0',5(3X,E14.6))
      WRITE(6,80)
   80 FORMAT('0',5X,'DISTANCE',10X,'TIME',5X,
     & 'THEORETICAL TIME',10X,'DIFF')
C
      STD=0.0
      DO 90 K=1,N
      DIFF=TY(K)-Y(K)
      STD=STD+DIFF**2
      WRITE(6,95) X(K),Y(K),TY(K),DIFF
   95 FORMAT('0',5X,F9.3,5X,F9.3,10X,F9.3,5X,F9.3)
   90 CONTINUE
C
      STD=STD/N
      WRITE(6,91) STD
   91 FORMAT('0',4X,'SQUARE NORM OF TIME IS',F9.6)
C
      CALL PLOTS
C
      CALL PLOTA(X,TIME,TY,N)
```

```
C
      N=43
      DO 93 K=1,N
   93 X(K)=(K-1)*5.0
C
      CALL ZVEL(X,N,0.2,C,LD,Z,VMAX)
      WRITE(6,154)
  154 FORMAT(8X,'DISTANCE',8X,'DEPTH',8X,'VMAX')
      DO 150 K=1,N
      WRITE(6,155) X(K),Z(K),VMAX(K)
  155 FORMAT('0',4X,3F12.4)
  150 CONTINUE
      CALL PLTA(Z,VMAX,N)
C
      STOP
      END
C
      SUBROUTINE PLOTA(X,Y,TY,N)
C
C     THIS SUBROUTINE PLOTS THE TIME-DISTANCE CURVE.
C
C     REQUIRED INPUTS
C     THE TITLES OF X- AND Y- AXIS
C     AXLEN-AYLEN: DESIRED LENGTH OF X AND Y AXIS
C     NTITLX-NTITLY: NUMBER OF CHARS IN X-AND Y-TITLES
C     X-Y: THE VECTORS TO BE PLOTTED
C     NDATA: NUMBER OF ELEMENTS IN VECTOR X OR Y
C
      DIMENSION X(2),Y(2),TY(2)
      COMMON AW
C
C  PLOT EVERY DATA POINT
      IREP=1
      AXLEN=5.0
      AYLEN=4.0
C
C  ENLARGE OR REDUCE THE SIZE OF THE ENTIRE PLOT
      CALL FACTOR(1.0)
C
C  MOVE ORIGIN IN A BIT TO ALLOW FOR LABELS
      CALL PLOT(1.0,11.0,-3)
C
C  SCALE THE INPUT VECTORS
C
      X(N+1)=0.0
      X(N+2)=44.0
      Y(N+1)=0.0
      Y(N+2)=10.0
C
C  PLOT X-AND Y- AXIS
      CALL AXIS(0.0,0.0,'DISTANCE KM',-11,AXLEN,0.0,
     & X(N+1),X(N+2))
      CALL AXIS(0.0,0.0,'TIME SEC',8,AYLEN,90.,Y(N+1),
     & Y(N+2))
```

```
      CALL SYMBOL(0.4,4.4,0.16,AW,0.0,30)
C
      CALL LINE(X,Y,N,1,0,3)
C      CALL LINE(X,TY,N,1,0,3)
      WRITE(6,10) X(N+1),X(N+2),Y(N+1),Y(N+2)
   10 FORMAT(' SCALE FACTOR ',4F15.2)
C
C  TERMINATE THE PLOT
      CALL PLOT(0.0,-4.6,-3)
      RETURN
      END
C
      SUBROUTINE PLTA(X,Y,N)
C
C     THIS SUBROUTINE PLOTS THE VELOCITY-DEPTH CURVE
C
C
      DIMENSION X(2),Y(2)
C
C  PLOT EVERY DATA POINT
      IREP=1

C
C
C  SCALE THE INPUT VECTORS
      AXLEN=5.0
      AYLEN=3.0
      X(N+1)=0.0
      X(N+2)=6.0
      Y(N+1)=5.0
      Y(N+2)=1.0
C
C  PLOT X-AND Y- AXIS
      CALL AXIS(0.0,0.0,'DEPTH KM',-8,AXLEN,0.0,
     & X(N+1),X(N+2))
      CALL AXIS(0.0,0.0,'VELOCITY KM/S',13,AYLEN,90.,
     & Y(N+1),Y(N+2))
C
      CALL LINE(X,Y,N,1,0,3)
C
C  TERMINATE THE PLOT
      CALL PLOT(0.0,0.0,999)
      RETURN
      END
C
C
      SUBROUTINE ZVEL(X,LX,DELX,C,LC,Z,VEL)
C
C     THIS SUBROUTINE EVALUATES THE WHB INTEGRAL AT ANY
C     ARBITRARY DISTANCE STARTING WITH A INITIAL VELOCITY
C     OF 5.30 KM/S.
C
      DIMENSION X(2),C(2),Z(2),VEL(2)
      ARCOSH(Y)=ALOG(Y+SQRT(Y**2-1.0))
```

```
C
      K1=1
      DO 10 KK=1,LX
      ORIG=X(1)
      XMAX=X(K1)-ORIG
      IF(XMAX.LE.0.0) GO TO 15
      SLOPE=DERV(C,LC,XMAX)
      VEL(K1)=1/SLOPE
      V=VEL(K1)
C
      N=XMAX/DELX
      ZZ=0.0
      X1=XMAX/N
      XX=X1
      DO 20 K=1,N
      SLOPE=DERV(C,LC,XX)
      ARG=V*SLOPE
      IF (K.EQ.N) ARG=1.0
      ZZ=ZZ+ARCOSH(ARG)*DELX
   20 XX=XX+X1
      GO TO 30
C
   15 VEL(K1)=5.30
      Z(K1)=0.0
      K1=K1+1
      GO TO 10
   30 Z(K1)=1/3.1416*ZZ
      K1=K1+1
   10 CONTINUE
      RETURN
      END
C
C
      REAL FUNCTION DERV(C,LC,X)
C
C     THIS FUNCTION CALCULATES THE DERIVATIVE AT ANY
C     POINT FROM THE POLYNOMIAL FUNCTION.
C
      DIMENSION C(LC)
C
      Y=C(2)
      DO 10 L=3,LC
   10 Y=Y+C(L)*(L-1)*X**(L-2)
      DERV=Y
      RETURN
      END
C
C
      SUBROUTINE REDUTI(LX,X,T,RT,RX)
C
C     THIS SUBROUTINE REDUCES THE TRAVEL-TIME DATA
C     DOWN TO THE BASE OF THE SURFACE LAYER
C
      DIMENSION X(2),T(2),RT(2),RX(2),V(2),DEPTH(2)
```

```
C
      IF (RT(3).LE.0.0) GO TO 100
      R1=(RT(1)-RT(2))/(RX(2)-RX(1))
      R2=(RT(3)-RT(2))/(RX(3)-RX(2))
C
      T(1)=0.0
      DO 10 I=2,LX
      TORIG=T(I)
      IF(X(I).LE.RX(2)) T1=R1*(RX(2)-X(I))+RT(2)
      IF(X(I).GT.RX(2)) T1=R2*(X(I)-RX(2))+RT(2)
      T(I)=T(I)-T1
      WRITE(6,20) X(I),TORIG,T(I),T1
   20 FORMAT('0','H1',4(F10.4,5X))
   10 CONTINUE
      GO TO 110
C
  100 R1=(RT(2)-RT(1))/(RX(2)-RX(1))
      T(1)=0.0
C
      DO 40 I=2,LX
      IF(X(I).LE.RX(2)) T1=R1*X(I)+RT(1)
      T(I)=T(I)-T1
C     WRITE(6,45) X(I),T(I),T1
C 45  FORMAT('0','H1',3F12.4)
   40 CONTINUE
  110 RETURN
      END
```